

Acknowledgements

We wish to thank the following individuals for their special assistance:

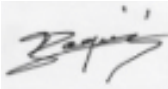
Dr. Daniel P. Schrage
Dr. Robert G. Loewy
Dr. Lakshmi Sankar
Dr. Jou-Young Choi
Hangil Chae
Chang Chen
Srinivas Jonnalagadda
CAPT Andy Bellochio

Academic Credit

All members of this design team received academic credit for this proposal. This design was the capstone project for AE6334, Rotorcraft Design II, a four-hour credit graduate course offered by Georgia Tech and instructed by Dr. Schrage.


2005 Georgia Tech Graduate Design Team

Aaron Pridgen (Masters Student)

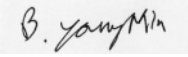


Ludvic Baquie (Masters Student)

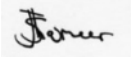
Alex Moodie (Ph. D. Student)



Mandy Goltsch (Ph. D. Student)



Byung-Young Min (Ph. D. Student)

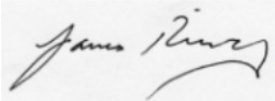


Sameer Hameer (Masters Student)

Dominic Scola (Masters Student)



Vivek Kaul (Masters Student)



James Rigsby (Ph. D. Student)

Executive Summary

The need for rapid vertical deployment of the Future Combat System (FCS) from ship to shore necessitates the generation of new designs in Heavy-Lift VTOL rotorcraft. Special considerations, such as their shipboard capability and performance constraints, were outlined in the 2005 Request For Proposal (RFP) as part of the 22nd Annual Student Design Competition sponsored by Boeing and AHS International. A graduate team from the Georgia Institute of Technology presents their results for the preliminary design of a configuration capable of performing all mission profile requirements and meeting all required system capabilities. The Georgia Tech Tandem (GTT) is their proposal for this competition.

The GTT was generated through a series of system level processes and analyses beginning with the decomposition of a clear problem statement. A measure of merit for designs and their comparison was created in an Overall Evaluation Criteria (OEC). Then an initial concept selection indicated that a tandem type rotorcraft would best meet the RFP requirements, and—through a detailed sizing and synthesis process utilizing the RF Method—the pure tandem configuration was chosen as the proposal candidate. Special consideration was made to justify and validate all the results that led to the GTT selection. Preliminary design of the GTT continued through the entire range of rotorcraft design disciplines as the selection of design parameters continued with greater fidelity. An aerodynamic analysis of the main rotor and hub design that included aircraft performance was performed. Then other aspects of the hub design were determined that included results of the blade dynamics. A broad structural design for the GTT is proposed as well as details for the aircraft's stability and control design. Additionally, the power plant selection and unique drive system design are presented. Finally, an evaluation of the GTT cost analysis is summarized. All the elements of GTT design combine to offer the best proposal for the Heavy Lift VTOL Aircraft requested in the 22nd Student Design Competition.

Table of Contents

ACKNOWLEDGEMENTS	I
ACADEMIC CREDIT	I
2005 GEORGIA TECH GRADUATE DESIGN TEAM	I
EXECUTIVE SUMMARY	II
TABLE OF CONTENTS	III
LIST OF TABLES	V
LIST OF FIGURES	VI
LIST OF ACRONYMS	VIII
LIST OF SYMBOLS	IX
COMPLIANCE MATRIX	X
1 INTRODUCTION	1
2 FUNCTIONAL ANALYSIS	1
2.1 FUNCTIONAL DECOMPOSITION	1
2.2 PROBLEM STATEMENT.....	3
3 AIRCRAFT CONFIGURATION TRADE STUDY	3
3.1 CONCEPT DEVELOPMENT	3
3.1.1 <i>Single Main Rotor</i>	3
3.1.2 <i>Tandem</i>	4
3.1.3 <i>Tilt Rotor</i>	4
3.1.4 <i>Quad Tilt Rotor</i>	5
3.1.5 <i>Slowed Rotor Compound</i>	5
3.2 PRELIMINARY CONCEPT ANALYSIS - OVERALL EVALUATION CRITERIA	6
3.3 TANDEM ROTOR TRADE-OFF STUDY	8
3.4 CONFIGURATION ANALYSIS	9
3.5 CONFIGURATION SELECTION – OEC ANALYSIS	11
4 PERFORMANCE	13
4.1 DRAG BUILDUP.....	14
4.2 PERFORMANCE ANALYSIS	15
4.3 AUTOROTATION.....	18
5 ROTOR DESIGN	20
5.1 ROTOR DIAMETER	20
5.2 TIP SPEED	20
5.3 BLADE AREA	21
5.4 SOLIDITY	21
5.5 BLADE TWIST AND TAPER	22
5.6 AIRFOIL DESIGN	23
5.7 BLADE TIP DESIGN	30
5.8 ROOT CUT-OUT.....	31
6 HUB DESIGN	31
6.1 SELECTION OF CANDIDATE HUB SYSTEMS	31
6.2 HINGE OFFSET AND POWER BLADE FOLDING	32
6.3 MATERIAL SELECTION.....	33
6.4 ROTOR HUB WEIGHTS AND PARTS COUNT	33
6.5 CONTROL POWER REQUIREMENTS	34
6.6 CONTROL POWER IN AUTOROTATION.....	34
6.7 PRECISION MANEUVERING/CARGO HANDLING	34

6.8	ROTOR DYNAMICS AND VIBRATION	35
6.9	SINGLE BLADE ANALYSIS	35
6.10	GROUND AND AIR RESONANCE	36
6.11	ADDITIONAL CONSIDERATIONS	37
7	STRUCTURAL DESIGN.....	37
7.1	STRUCTURAL CRITERIA	37
7.2	GEOMETRY	37
7.3	MATERIALS	38
7.4	WEIGHT AND BALANCE.....	39
7.5	DESIGN FLIGHT SPEEDS.....	41
7.6	LOAD FACTORS	41
7.7	V-N DIAGRAM.....	42
7.8	BLADE STRUCTURAL DESIGN	42
7.8.1	<i>Blade</i>	42
7.8.2	<i>Root End Retentions and Tip Closure</i>	42
7.9	ALIGHTING GEAR	43
7.10	LOAD HANDLING.....	44
7.11	FATIGUE	44
8	STABILITY AND CONTROL.....	45
8.1	REQUIREMENTS	45
8.2	STABILITY ANALYSIS	47
8.2.1	<i>Methods Description</i>	47
8.2.2	<i>Trim Analysis</i>	48
8.2.3	<i>Linearized System Results</i>	48
8.2.4	<i>Eigenvalue Analysis</i>	49
8.2.5	<i>Static Stability Analysis</i>	49
8.3	FLIGHT CONTROL SYSTEM	50
8.4	MAINTAINABILITY	50
9	ENGINE SELECTION	51
9.1	ENGINE DETAILS	51
9.2	ENGINE INSTALLATION AND POWER LOSSES	52
10	TRANSMISSION	53
10.1	SINGLE SPEED TRANSMISSION	54
10.2	TWO SPEED TRANSMISSION.....	55
10.3	STRESS ANALYSIS	56
10.3.1	<i>Geometry Factors</i>	56
10.3.2	<i>Force Analysis</i>	57
10.3.3	<i>Stress Analysis</i>	57
10.4	SHAFT ANALYSIS.....	58
11	COST ANALYSIS	58
12	CATIA DRAWINGS	59
12.1	3 VIEW.....	59
12.2	ISOMETRIC VIEW	60
12.3	INTERNAL LAYOUT.....	61
13	REFERENCES	62

List of Tables

TABLE 1: VARIABLES - HARRIS COST MODEL.....	7
TABLE 2: AIRCRAFT CONFIGURATION SELECTION	7
TABLE 3: TANDEM ROTOR FAMILY TRADE-OFF STUDY DATA	12
TABLE 4: GEORGIA TECH TANDEM AERODYNAMIC DATA.....	14
TABLE 5: DRAG ESTIMATION METHOD VALIDATION	15
TABLE 6: FLAT PLATE DRAG AREA ESTIMATION OF GTT (GW:105,334 LBS).....	15
TABLE 7: TRADE STUDY FOR TWIST ANGLE AND TAPER RATIO.	23
TABLE 8: RANGE OF ANGLE OF ATTACK AND MACH NUMBER FOR NEW AIRFOIL DESIGN.....	25
TABLE 9: ROTOR HUB CANDIDATE CONFIGURATIONS	32
TABLE 10: ADVANTAGES OF ELASTOMERIC COMPONENTS [14].....	33
TABLE 11: SYMMETRICAL AND ASYMMETRICAL FLIGHT MANEUVERS [7]	37
TABLE 12: GEORGIA TECH TANDEM GEOMETRY	38
TABLE 13: PUGH MATRIX OF CANDIDATE MATERIALS	38
TABLE 14: ALUMINUM ALLOY COMPARISON.....	39
TABLE 15: CONCEPT MATERIALS.....	39
TABLE 16: COMPONENT WEIGHT	40
TABLE 17: LONGITUDINAL C.G. CALCULATION.....	40
TABLE 18: DESIGN FLIGHT SPEEDS.....	41
TABLE 19: LOAD FACTOR	41
TABLE 20: ROLL OVER ANGLES.....	44
TABLE 21: STABILITY AND CONTROL REQUIREMENTS.....	46
TABLE 22: MODEL ASSUMPTIONS	46
TABLE 23: STATIC STABILITY ANALYSIS	49
TABLE 24: ENGINE DATA	51
TABLE 25: AE-1107C SPECIFICATION [20,21].....	52
TABLE 26: POWER LOSS ESTIMATION [7]	52
TABLE 27: POWER AND TORQUE RESULTS	53
TABLE 28: GEAR PARAMETERS.....	55
TABLE 29: GEAR RATIO AND TORQUE	55
TABLE 30: TWO SPEED TRANSMISSION RESULTS	56
TABLE 31: GEAR DIAMETER	56
TABLE 32: GEOMETRY FACTORS.....	57
TABLE 33: FORCE ANALYSIS RESULTS.....	57
TABLE 34: CONTACT AND BENDING STRESSES	57

List of Figures

FIGURE 1: OPERATIONAL ARCHITECTURE OF THE FUTURE FORCE	1
FIGURE 2: GENERALIZED SYSTEM FUNCTIONAL ARCHITECTURE.....	2
FIGURE 3: FUNCTIONAL ARCHITECTURE (MISSION PROFILE DIAGRAMS)	3
FIGURE 4: MODEL CENTER© TANDEM ROTORCRAFT WIRE DIAGRAM.....	8
FIGURE 5: VEHICLE SIZING METHODOLOGY	9
FIGURE 6: GROSS WEIGHT VS DISK LOADING.....	10
FIGURE 7: CRUISE SPEED VS DISK LOADING.....	10
FIGURE 8: INSTALLED HP VS DISK LOADING.....	10
FIGURE 9: ACQUISITION COST (\$MIL) VS DISK LOADING.....	10
FIGURE 10: VALUE (OEC) VS DISK LOADING.....	10
FIGURE 11: OEC HP, EMPTY WEIGHT, AND CRUISE SPEED.....	12
FIGURE 12: ACQUISITION COST, CRUISE SPEED (OEC).....	13
FIGURE 13: AC, CRUISE SPEED (OEC) II.....	13
FIGURE 14: DRAG LOADING OF GTT WITH HISTORICAL DATA [4].....	15
FIGURE 15: POWER REQUIREMENTS.....	16
FIGURE 16: HOVER CEILING.....	16
FIGURE 17: HOVER CHART.....	17
FIGURE 18: FORWARD FLIGHT PERFORMANCE.....	18
FIGURE 19: PAYLOAD-RANGE DIAGRAM	18
FIGURE 20: AUTOROTATION INDICES	19
FIGURE 21: AUTOROTATION LANDING CHARACTERISTICS.....	19
FIGURE 22: SOLIDITY BOUNDARIES	22
FIGURE 23: DIMENSIONLESS BLADE LIFT ALONG THE BLADE RADIAL DIRECTION FOR DIFFERENT TWIST ANGLE.....	23
FIGURE 24: ROBUST DESIGN PROCEDURE FOR ROTORCRAFT AIRFOIL.....	24
FIGURE 25: ANGLE OF ATTACK AND LOCAL MACH NUMBER DISTRIBUTION.....	25
FIGURE 26: IN-HOUSE CFD CODE VALIDATION WITH NACA0012 EXPERIMENTAL DATA FROM AGARD.....	26
FIGURE 27: XFOIL AND IN-HOUSE CFD CODE VALIDATION WITH NACA0015.....	26
FIGURE 28: NEW AIRFOIL SHAPE, GTHLH1 ($0.5 \leq r/R \leq 0.8$), GTHLH3 ($0.8 \leq r/R \leq 1.0$).....	26
FIGURE 29: VR7 AND GTHLH1 PERFORMANCE (XFOIL SOLUTION).....	27
FIGURE 30: VR8 AND GTHLH3 PERFORMANCE IN ADVANCING SIDE (IN-HOUSE CODE EULER SOLUTION).....	28
FIGURE 31: PRESSURE CONTOURS AT THE ADVANCING BLADE TIP	28
FIGURE 32: NEW AIRFOIL LIFT COEFFICIENTS.....	28
FIGURE 33: GTT ROTOR BLADE DETAILS.....	29

FIGURE 34: BLADE TIP DESIGN	30
FIGURE 35: NOTIONAL GT ROTOR HUB CONFIGURATION.....	32
FIGURE 36: TYPICAL ELASTOMERIC SPHERICAL BEARING	33
FIGURE 37: SINGLE BLADE ANALYSIS FAN PLOT.....	36
FIGURE 38: LONGITUDINAL CENTER OF GRAVITY ENVELOPE.....	40
FIGURE 39: COMPONENT CENTER OF GRAVITY.....	41
FIGURE 40: V-N DIAGRAM.....	42
FIGURE 41: BLADE STRUCTURE	43
FIGURE 42: FRONT AND AFT ALIGHTING GEAR	43
FIGURE 43: FCS LOADING CONFIGURATION.....	44
FIGURE 44: FRONT AND AFT ALIGHTING GEAR	45
FIGURE 45: TRIM ANALYSIS RESULTS.....	48
FIGURE 46: ROOT LOCUS	49
FIGURE 47: CONTROLLER ARCHITECTURE	50
FIGURE 48: AE-1107C ENGINE [20]	52
FIGURE 49: FOUR ENGINE COMBINER BOX.....	53
FIGURE 50: PLANETARY GEAR ARRANGEMENT	54

List of Acronyms

ACAH	Attitude Command Attitude Hold
AFP	Air Force Turboprop
AFS	Air Force Turboshaft
AFF	Air Force Turbofan
AGARD	Advisory Group for Aerospace Research & Development
AGMA	American Gear Manufacturers Association
AI	Autorotation Index
BERP	British Experimental Rotor Program
CAS	Control Augmentation System
CFD	Computational Fluid Dynamics
CG	Center of Gravity
CRP	Contingency Rated Power
CVN	Nuclear Aircraft Carrier
DOE	Design of Experiments
DOF	Degrees of Freedom
EW	Empty Weight
FADEC	Full Authority Digital Engine Control
FCS	Flight Control System
FCS	Future Combat System
FM	Figure of Merit
FMR	Figure of Merit Ratio
FPS	Feet Per Second
GPS	Global Positioning Satellite
GT	Georgia Tech
GTT	Georgia Tech Tandem
GW	Gross Weight
HLH	Heavy Lift Helicopter
HP	Horse Power
IFR	Instrument Flight Reference
IRP	Intermediate Rated Power
MCAA	Model Center Analysis Approach
MCP	Max. Continuous Power
MRP	Military Rated Power
NURBS	Non-Uniform Rational B-Spline
OEC	Overall Evaluation Criteria
OEI	One Engine Inoperative
PD	Preliminary Design
RALI	Relative Autorotational Landing Index
RCRH	Rate Command Rate Hold
RFP	Request for Proposal
RPM	Revolutions per Minute
S&C	Stability and Control

SAS	Stability Augmentation System
SFC	Specific Fuel Consumption
SHP	Shaft Horse Power
SL	Sea Level
TOGW	Take Off Gross Weight
UA	Unit of Action
UE	Unit of Employment
VFR	Visual Flight Reference
VTOL	Vertical Take Off and Landing

List of Symbols

a	Lift Curve Slope
c	Chord
DBL	Dimensionless Mean Blade Lift
EW	Empty Weight
L'	Lift per Unit Span
n	Load Factor
R	Radius
R/C	Rate of Climb
R/D	Rate of Descent
R _{FA}	Fuel available
R _{FR}	Fuel required
TR	Taper Ratio
ρ	Density
Ω	Rotational Speed

Compliance Matrix

General System Requirements	Section
Dual piloted, VTOL aircraft	2.1, 3.2, 3.5
Initial Operational Capability (4 delivered aircraft) in year 2018	11
Anticipated fleet size of 200 aircraft over 15 year manufacturing period	11
Intra-theater deployment of 1000 nm range without refueling	3.3, 4.2
Mission Profile Requirements	Section
Aircraft mission performance sized to the sea-basing concept	3.3, 3.4, 12.1
Aircraft sizing trade study based on mission profile @ ISA+20°C	3
Mission profile: - Warm-up (10 min at idle at sea level) - Shipboard takeoff (1 min HOGE plus additional time for external load) - Climb (sea level to 3000') - Cruise (99% best range speed for outbound radius w/external drag as app) - Loiter (15 min near LZ for mission cueing) - LZ ops (3 min HOGE at 3000' plus time for vehicle unloading) - Cruise inbound (99% best range speed) - Shipboard landing (2 min HOGE at sea level) - Reserve (land with 20 min. loiter fuel at 500 feet) - Prepare and refuel for follow on mission	RFP, 3.3, Figure 4
System Capability Requirements	Section
High value technologies in: - Airframe - Propulsion - Cargo handling - Aircraft human factors engineering	7.3, 9.1, 6.7, 8.3
Ship compatible with L-Class and/or CVN to include: - Deck operations with other aircraft - Maintenance and support issues - Meets hangar deck access limits of maximum folded height - Meets elevator size limits - Meets elevator weight limits	12.1, 2.1, 3.3, 6.2, 7.2
Transport at least (2) 463L fully-loaded pallets (88"x108" footprint plus netted loads up to 96" high and up to 10,000 lbs)	3.3, 4.2
Be able to transport a 20 ton FCS combat ready vehicle: - Fits in C-130 cabin cross section (102"high x 107" wide) x 240" long - Tracked or wheeled compatible - Attachment points available for internal or external load carriage	12.1, 3.2, 3.3, 4.2, 7.2, 7.4,
Power-off glide/autorotation to a survivable emergency landing	4.3, 6.6, 7.9
Powered rotor blade (and airframe) folding for elevator and/or hanger deck access	6.2
Minimum normal load factor structural capability at design takeoff gross weight of -0.5g to +2.5G	7, 7.7

System Capability Requirements (Continued)	Section
Minimum sustained turn rate capability at cruise speed of 2x standard rate turn	5, 6.5, 8.2.2
OEI, HOGE at 60% fuel and full payload using no more than emergency power at sea level, ISA+20°C ambient conditions	3, 4
Flight crew of three, with side-by-side cockpit (pilot and copilot) seating, and cabin seating for a crew chief	RFP, 7.4, 12.1, 12.3
Accommodation for FCS vehicle crew of 2	RFP, 2.1, 7.2, 7.4, 12.1
Cabin oxygen or pressurization if sustained cruise above 10,000' pressure altitude	7.4
Missile warning systems and countermeasures (RF and IR)	2.1, 7.4
Mission equipment suite (navigation, sensors, communication gear, etc.) suitable to perform flight operations in adverse weather conditions	7.4
Access for inspection and rapid repair/replacement of all aircraft components (engines, transmissions, avionics, flight controls, hydraulic, electrical, fuel, cooling systems, etc.)	6.1, 8.4
Good crashworthiness design: Landing gear struts that do not penetrate the cabin area. High mass items (engine and transmissions) that have adequate crash protection to prevent entry into the cabin areas. Crashworthy fuel tanks Adequate seat stroke (at least 8 inches).	4.3, 6.6, 7.9
Assumption of emerging turbo shaft engine technology levels, including IHPTET III technologies	9.1, 9.2
Additional Detail	Section
Structural Design, including materials, must be described.	7
Describe analysis methods and the results of the flight performance, S&C, and handling qualities evaluations	4, 6, 8
Description of the engine installation and drive system	9, 10
Manufacturing approaches and risks for non-traditional hardware designs	5, 6, 7, 10
Optional discipline of specific interest	3.3, 3.5, 6.8-6.10, 10

1 Introduction

As the United States military evolves to meet the changing requirements in the combat theater the need for heavy lift VTOL aircraft has arisen. Further more a ship to shore capable transport that does not rely on fixed airbases and can rapidly deliver equipment is desired for the future emphasis of flexible mission basing. The objective of this report is to develop a preliminary design concept of a heavy lift VTOL aircraft that is shipboard compatible and capable.

2 Functional Analysis

In order to better understand our customer requirements we utilized a process known as functional analysis. The purpose of this systems engineering process is to “*transform the functional, performance, interface and other requirements that were identified through requirements analysis into a coherent description of system functions*” [1] that can be used to guide subsequent design synthesis activities.

2.1 Functional Decomposition

It stands to reason that functional and performance requirements at any level in a system are derived from higher-level requirements. For this reason we were able to decompose major system functions to define successively lower-level functional and performance requirements, thus defining architectures at ever-increasing levels of detail [1].



FIGURE 1: OPERATIONAL ARCHITECTURE OF THE FUTURE FORCE

Initially we returned to the requirements outlined in the RFP and were able to construct an operational architecture diagram depicting how our aircraft is expected to operate within the operational environment of the future force. From the Operational Architecture depicted in Figure 1, we determined that the Heavy Lift VTOL aircraft of the future will operate within the operational and tactical environment occupied by units of employment (UEs) and units of action (UAs). In addition, it has a sea-borne requirement that necessitates an employment partnership with Amphibious Assault ships (L-Class) and aircraft carriers (CVN) of the Navy and Marine Corps. From this information we were able to construct a generalized functional architecture diagram specific to our aircraft.

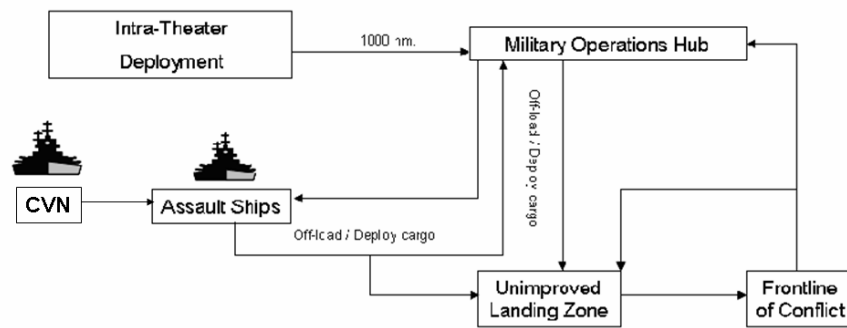


FIGURE 2: GENERALIZED SYSTEM FUNCTIONAL ARCHITECTURE

Now that we know the operational and tactical environment in which our system is intended to operate, it is important to understand what exactly is expected of our aircraft from a “mission accomplishment” standpoint. To this end, we synthesized the information from Figure 1 and Figure 2 with mission data provided in the RFP and conducted an additional level of functional decomposition. Finally, we produced functional architecture diagrams - specific to our aircraft and the mission it is intended to perform - in the form of mission profile diagrams.

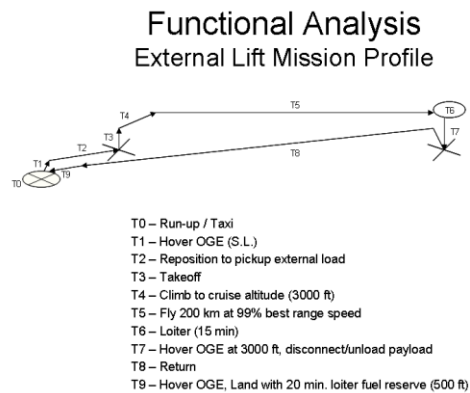
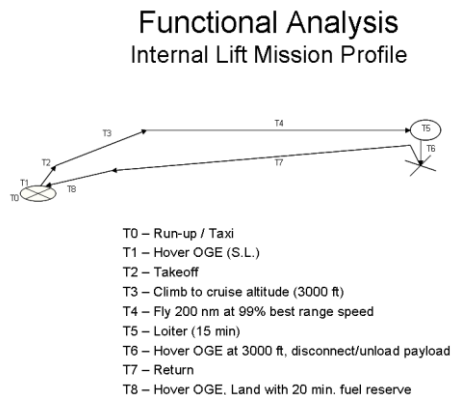


FIGURE 3: FUNCTIONAL ARCHITECTURE (MISSION PROFILE DIAGRAMS)

2.2 Problem Statement

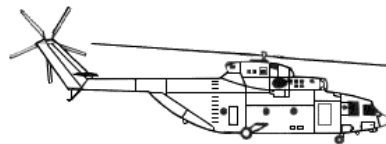
At the conclusion of the requirements and functional analysis stage of the design process we were able to formulate a clear, concise, and well-crafted problem statement.

Transport light combat vehicles (FCS systems), via vertical envelopment tactics, over military ranges of interest into hostile, unimproved terrain in order to swiftly engage and decisively defeat enemy forces. Movement will be initiated from a land or sea-based point of debarkation, conducted as swiftly as possible, and vehicles will arrive in a ready-to-fight configuration.

3 Aircraft Configuration Trade Study

3.1 Concept Development

Once we developed a comprehensive understanding of the mission our aircraft is intended to perform, we were in a better position to develop design alternatives. At this stage, we conducted several brainstorming exercises during which every member of the design team was asked to propose possible concepts and aircraft configurations to meet the requirements outlined in the RFP. We considered this our “first cut” at generating feasible alternatives. Our goal in this stage was to conduct unconstrained brainstorming and attempt to adequately represent every major solution no matter how impractical some may have seemed at first. Our list of initial concepts consisted of the following five aircraft configurations.



3.1.1 Single Main Rotor

The single main rotor configuration consists of a single main rotor and an appropriate anti-torque device. Historically, this conventional helicopter design is limited in forward flight by the aerodynamic and propulsive limitations of the main rotor (compressibility effects and retreating blade stall). In addition, there is high parasite

drag associated with the main rotor hub, which contributes to a poor overall lift-to-drag ratio of the aircraft. Without modification (through compounding), the conventional helicopter is limited to a cruise speed of approximately 150 knots [5].



3.1.2 Tandem

The classic tandem rotor configuration consists of two counter-rotating main rotors positioned one in front of the other along the longitudinal axis of the airframe. An advantage of the tandem rotor design is the elimination of the need for an anti-torque device. As a result there is a savings in design weight and complexity. More importantly, the tandem rotor aircraft is based upon a proven design and has been successfully employed in global heavy lift operations under harsh operating conditions for decades. The tandem rotor configuration traditionally allows for higher cruise speeds than the single main rotor design and has proven to be a stable platform for operations that may experience large C.G. travel.



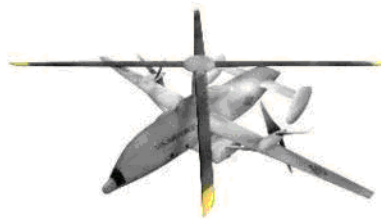
3.1.3 Tilt Rotor

The tilt-rotor aircraft takes-off and lands vertically through the use of two wing mounted main rotors. Once aloft, the aircraft goes through a conversion process in which the engines and rotors are progressively tilted forward until it has the approximate performance, and aerodynamic characteristics, of a turboprop airplane. The tilt-rotor design increases cruise speed to approximately 300 knots; however, it pays a significant penalty in empty weight and complexity due to the conversion mechanism. In addition, due to the fact that the propellers cannot be as large as a traditional helicopter rotor, poor hover efficiency and high disk loading hinder the tilt rotor.



3.1.4 Quad Tilt Rotor

Through the addition of a second set of wings, engines, and rotors/propellers, the quad tilt-rotor is able to improve the lifting capacity and velocity of the traditional tilt rotor design. The quad tilt-rotor has the same considerations that include the weight, complexity, poor hover efficiency, and high disk loading as with the tilt rotor.



3.1.5 Slowed Rotor Compound

As stated previously, compounding is a technique used to improve the aerodynamic and performance characteristics of the single main rotor design. Through the addition of auxiliary lifting surfaces and propulsive devices the forward airspeed of the traditional helicopter can be increased beyond the limits of what is currently possible. As will be mentioned further, it was the intent of our design group to explore the effects of adding a “slowed”, or “variable speed”, rotor to the classic compound helicopter configuration too. We can further increase the cruise speed of this design by slowing the rotational speed of the main rotor in high-speed forward flight. However, we have come to realize in helicopter design that “there is no free lunch”. Similar to the situation of the tilt-rotor and quad tilt-rotor designs, for increased performance we pay a significant penalty in added weight and system complexity. In addition, hover performance is reduced by the download of the rotor on the wing/auxiliary lifting surfaces.

3.2 Preliminary Concept Analysis - Overall Evaluation Criteria

One should always evaluate a decision by weighing available options against implicit or explicit evaluation criteria, particularly in this design. These criteria were specifically stated in the RFP as, “*the primary measure of merit will be the timeline for one aircraft to deliver (4) FCS combat vehicles versus the predicted acquisition cost of the aircraft.*” Based on this guidance, our Overall Evaluation Criteria (OEC) would be represented as

$\frac{\text{Mission Time}}{\text{Acquisition Cost}}$. From the previously mentioned mission/functional analysis and the assumption that our heavy lift

aircraft will be CVN “compatible” and L-Class “capable”, we have constructed the OEC as follows:

$$OEC = \frac{\left((2) \left(\frac{75nm}{V_{Cruise}} \right) - (4)(UploadTime) - (4) \left(\frac{125nm}{V_{Load}} \right) - (4)(DownLoadTime) - (4) \left(\frac{125nm}{V_{Cruise}} \right) - (3)(FuelTime) \right)}{AcquisitionCost}$$

EQUATION 1: OVERALL EVALUATION CRITERIA

As one can see from the OEC above, to maintain the convention that a larger OEC value is “better” we took the inverse of the mission time. Acquisition Cost was calculated using the Harris model—a price estimating relationship presented during the NASA Ames Research Center Economic Workshop 7-8 May 1996. This traditional price estimating relationship was developed through the careful analysis of decades of empirical aircraft data. Ultimately, it calculates aircraft cost as a function of numerous design factors (Equation 2). Appropriate values for several of the variables are provided in Table 1.

$$\text{Base Price} = \$227 \cdot H \cdot (\text{Empty Weight})^{0.4638} \cdot (\text{Horse Power})^{0.6238} \cdot (\text{Blades - Rotor})^{0.1750}$$

$$H = (\text{Engine Type}) \cdot (\text{Engine Number}) \cdot (\text{Country}) \cdot (\text{Rotors}) \cdot (\text{Landing Gear})$$

EQUATION 2: ACQUISITION COST (HARRIS COST MODEL)

From the Harris Cost model and our mission analysis we were able to calculate an OEC index for each of the five competing aircraft configurations. The OEC value was calculated based on actual design specifications and performance data for legacy aircraft and on estimated specs for future concepts (Quad Tilt Rotor and Slowed Rotor Compound). To eliminate possible bias in these calculations, upload and download times were kept consistent for

each configuration and were based off conservative estimates for internal vehicle loading. Table 2 presents the results of this analysis. From the table, the Tandem Rotor concept proved the best configuration. It was this configuration that we carried forward for further exploration and eventually through the preliminary design process.

TABLE 1: VARIABLES - HARRIS COST MODEL

Engine Type		Engine Number		Country		Number of Rotors	
Piston	1.000	Single	1.000	U.S.	1.000	Single	1.000
Piston Supercharged	1.330	Multi	1.328	Russia	0.337	Twin	1.084
Piston Converted to Turbine	1.175			France Germany	0.879	Landing Gear	
Gas Turbine	1.750			Italy	1.042	Fixed	1.000
				U.S. Military	0.804	Retractable	1.104

TABLE 2: AIRCRAFT CONFIGURATION SELECTION

	Upload Time	V_{Load}	Download Time	V_{Cruise}	Mission Time, hrs	AC (SMIL)	OEC	Rank	PER US \$
Single Main Rotor	20	152	10	165	10.31	66.74	0.1567	2	66,740,000
Advanced Tandem	20	175	10	180	8.22	55.23	0.2424	1	55,230,000
Tilt Rotor	20	200	10	300	7.08	64.62	0.2406	3	64,620,000
Quad Tilt Rotor	20	225	10	300	6.81	111.3	0.1484	4	111,300,000
Slowed Rotor Compound	20	365	10	400	5.41	140.9	0.1523	5	140,900,000

Though the Tandem concept proved to be the best configuration (based on our OEC), it was the team's desire to infuse state-of-the-art technology into the traditional Tandem Rotor design and investigate improved performance. Therefore, after initial concept selection of the Tandem concept, we conducted a more detailed trade-off study of the Tandem "Family" of design alternatives. In this study four variations of the Tandem Rotor aircraft were compared (Pure Tandem, Tandem Rotor Compound, Tandem Compound with Variable Speed Rotor, and the Tandem Tilt Wing with Variable Speed Rotor) based on preliminary performance calculations. The results of this study follow.

3.3 Tandem Rotor Trade-off Study

In order to conduct a thorough analysis of the various configurations in the Tandem Rotor aircraft “family” we utilized an interactive computer environment known as Model Center©. Through Model Center© we constructed our own model of a generic tandem rotor aircraft which, through a series inputs, could be easily modified to represent each of the configurations in the tandem rotor family. Utilizing the model we created, we performed vehicle sizing and calculated both initial performance data and OEC index values for the various designs. This OEC information allowed us to compare design results and ultimately focus on maximizing the OEC for chosen concept.

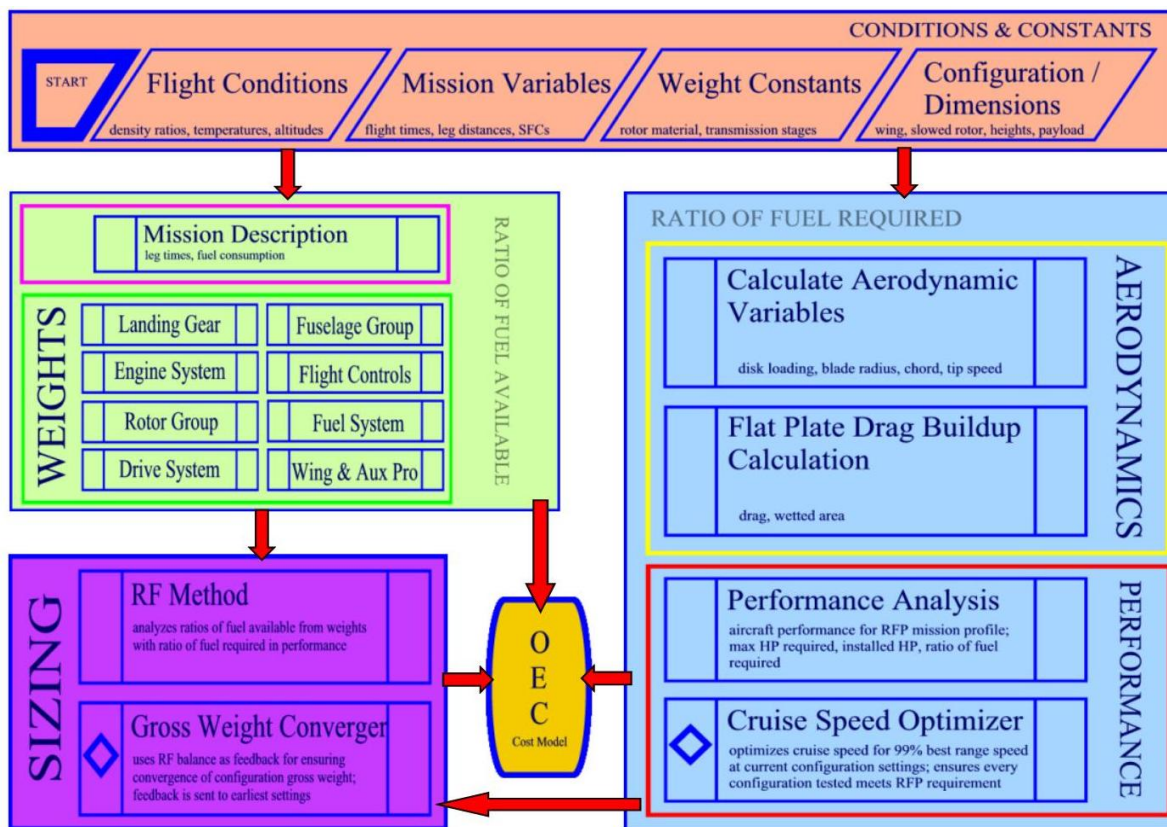


FIGURE 4: MODEL CENTER© TANDEM ROTORCRAFT WIRE DIAGRAM

The vehicle sizing and synthesis code in this model was based on the fuel balance method, also known as the “RF” method. Through the RF method an initial “guess” is made at the gross weight of the aircraft. From this initial gross weight estimate, performance values are calculated based on the mission profile of our vehicle. Next, the empty weight of the vehicle is determined and we ensure that the fuel required to accomplish the mission (at the

mission gross weight), R_{FR} , is equal to the fuel available (R_{FA}) at this empty weight. If the ratios are not equal, the configuration is not a viable solution. A new gross weight is entered according to feedback from the RF method and the process is iterated until convergence. Finally, because of its significant impact on vehicle sizing and performance, we chose disk loading as leading design parameter to generate a range of viable solutions. This range of solutions accurately represents the distribution of OEC for the specific configuration being analyzed. Therefore, we interpreted the optimum design as the combination of disk loading and maximum OEC that best meets the needs of the customer. A diagram of our sizing model is shown in Figure 5. Note that the power of the RF method lies in the fact that it is based upon specific mission requirements and can be tailored to various mission profiles. The Tandem sizing model we created ensures that all the mission profile requirements are met. An example of the decision strategy of the model sizing methodology is presented in Figure 5.

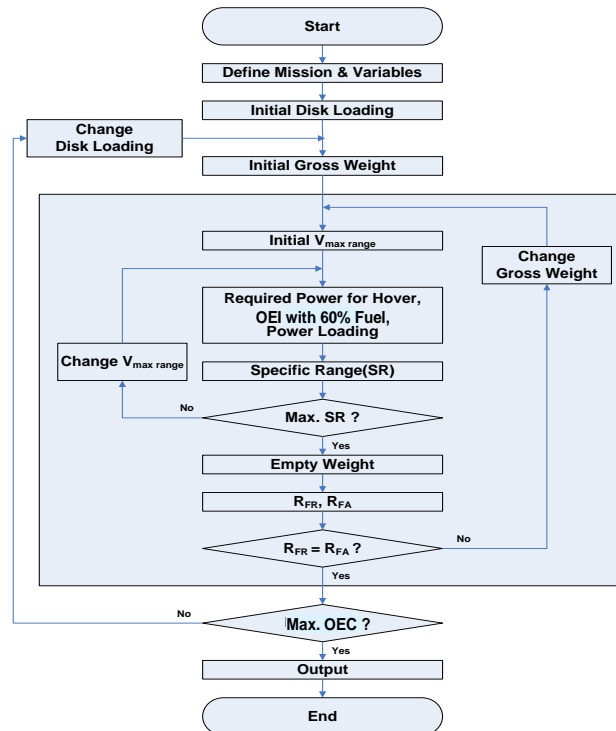


FIGURE 5: VEHICLE SIZING METHODOLOGY

3.4 Configuration Analysis

During the Tandem trade-off study, we varied disk loading for each configuration type and generated plots of weight, cruise speed, installed horsepower (HP), acquisition cost, and value (OEC) as a function of disk loading.

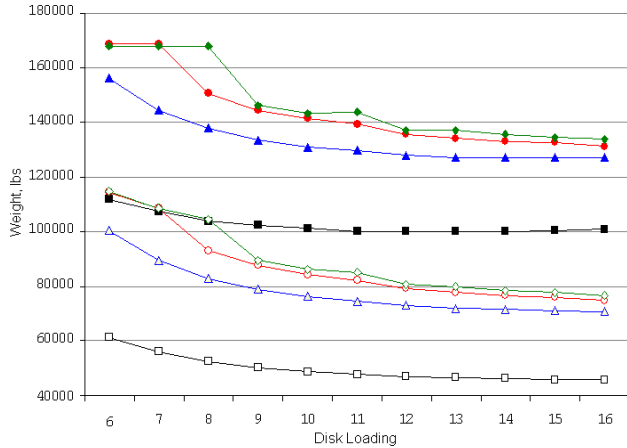


FIGURE 6: GROSS WEIGHT VS DISK LOADING

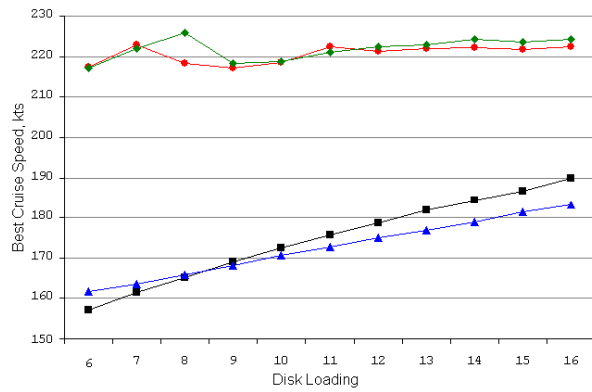


FIGURE 7: CRUISE SPEED VS DISK LOADING

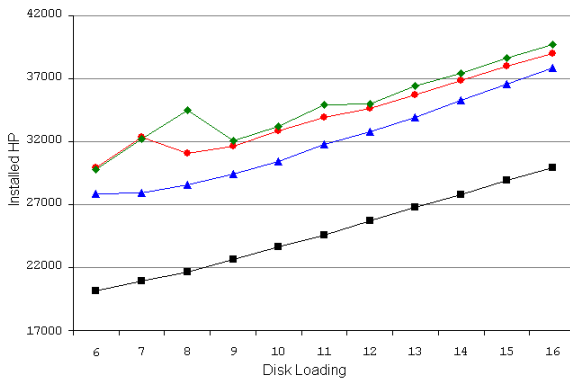


FIGURE 8: INSTALLED HP VS DISK LOADING

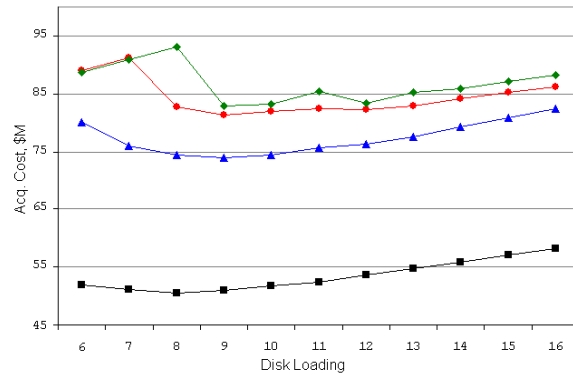


FIGURE 9: ACQUISITION COST (\$M) VS DISK LOADING

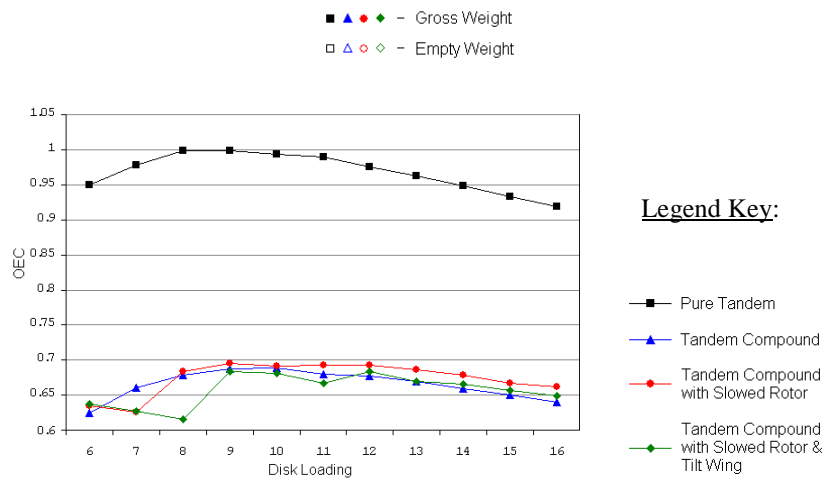


FIGURE 10: VALUE (OEC) VS DISK LOADING

From Figure 6 above, the pure tandem configuration provides the minimum gross weight. Specifically, at various disk loading values the pure tandem aircraft operates at gross weights approximately 25,000 lbs lighter than

the closest competitor (tandem compound). Being that the primary measure of merit is the timeline for one aircraft to deliver four FCS vehicles, the sizing model we created automatically optimized the best range speed for each configuration for a maximum cruise speed. With regards to cruise speed, 99% best range speed (as specified in the RFP), the slowed-rotor compound tilt-wing and the slowed-rotor compound configurations provide comparable performance with max cruise speeds of 223 knots (kts) and 221 kts, respectively and a common disk loading value of 12 lbs/ft². The pure tandem configuration provides a max cruise speed of 169 kts at a disk loading of 9 lbs/ft² and the tandem compound cruises at 171 kts at a disk loading of 10 lbs/ft². With regards to value, the pure tandem is the best configuration with an OEC index of 1. The next best configuration is the slowed-rotor compound concept with an OEC index of 0.7. The pure tandem has an OEC index of 1 because all the OEC values were normalized with the best OEC from the pure tandem.

3.5 Configuration Selection – OEC Analysis

It was apparent that the best configuration to meet the requirements outlined in the Request for Proposal (RFP) was the pure tandem helicopter. The pure tandem provided the minimum gross weight solution coupled with an impressive cruise speed of 169kts at a reasonable disk loading of 9 lbs/ft². Furthermore, in accordance with our OEC, it was by far the best value (a full 30% better than its closest competitor). It was somewhat surprising that the pure tandem configuration proved to be the best solution compared to more advanced aircraft designs like the slowed-rotor compound tilt-wing. Therefore, we began taking a closer look at the OEC and revisiting the mission profile to justify why we concluded with such results. We felt it necessary to justify the design through the OEC before taking the pure tandem configuration through the preliminary design process. The results of this investigation into the OEC are presented here.

As stated previously, the OEC is a function of time over Acquisition Cost. Furthermore, Acquisition Cost was estimated using the Harris Cost model, which is primarily a function of Aircraft Empty Weight and Installed Horse Power. In Figure 6 through Figure 10 above, one can see that though the pure tandem design does not provide the highest cruise speed, it is significantly lighter than all other options. Therefore, the pure tandem aircraft has a lower gross weight, requires less installed power, and resultantly has a significantly lower Acquisition Cost (almost half the price of the compound slowed-rotor tilt-wing). Simply stated, all other designs add complexity and weight, require additional installed power, incur a substantial increase in acquisition cost, and do not increase airspeed enough (i.e. decrease FCS delivery time) to justify the added cost. This became apparent when we conducted a

sensitivity study to assess the impact of increasing airspeed, or decreasing acquisition cost, on the OEC index. Through this study we found that increasing the airspeed of a configuration by 5kts improves the OEC to the same degree as keeping the airspeed constant and decreasing the acquisition cost by \$2MIL. Table 3 shows that the difference in airspeed between the slowest and fastest concept is 54kts. In order for the fastest concept (slowed-rotor compound tilt-wing) to be cost effective (in accordance with the OEC) we can only allow a cost increase of \$22MIL. The difference in cost between the slowest and fastest concept is \$32.4MIL

TABLE 3: TANDEM ROTOR FAMILY TRADE-OFF STUDY DATA

	GW	DL	Best Cruise Speed	ϕ	Installed HP	Total Mission Time, hrs	Acquisition Cost, Mio \$	OEC	Rotor Radius, ft	Blade Chord, ft	Body Dimension LxWxH	Flat Plate Area
Pure Tandem	102,209	9	169	0.491	22,633	9.40	51.0	1	45.3	2.81	71.8x15x15	78.8
Tandem Compound	130,810	10	171	0.582	30,442	9.36	74.4	0.688	48.6	3.35	76.2x15x15	89.1
Tandem Compound SR	135,817	12	221	0.584	34,650	8.42	82.2	0.692	45.2	3.75	71.8x15x15	87.2
Tandem Tilt Wing SR	137,123	12	223	0.589	34,966	8.40	83.4	0.684	45.5	3.77	72.2x15x15	87.5

In addition, the mission profile requirements do not support more complex designs. The mission is to deliver four FCS vehicles from an L-Class Assault Vessel, located 25nm offshore, to a landing zone located 100nm inland. Throughout the mission the tactical distances are relatively short (125nm legs to-and-from the L-Class). Assuming constant upload, download, and refuel times, the fastest configuration, cruising at an airspeed of 223kts (54kts faster than the slowest configuration), would successfully accomplish the mission in 8hrs and 24min; 1 hour faster than the slowest configuration. It hardly seems reasonable to pay close to twice the price (\$32.4MIL per aircraft) for a 1-hour savings over a 9.5-hour mission day. Table 3 lists the design specifications of the best OEC of each type calculated through the Tandem trade study.

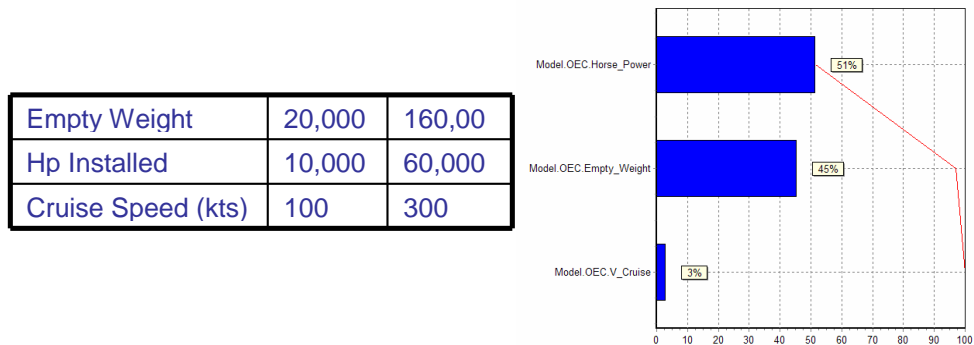


FIGURE 11: OEC HP, EMPTY WEIGHT, AND CRUISE SPEED

As part of this trade-off study we conducted a sensitivity analysis and design of experiments (DOE) to determine how the most important design characteristics affect the OEC. The figures and analysis presented support our justification of the OEC and our Tandem trade-off study results.

Figure 11 compares the effects of installed HP, empty weight (WE), and cruise speed (99% best range speed) in the OEC. HP contributes 51%, EW 45%, and cruise speed a mere 3%. What this tells us is that increasing the cruise speed of the vehicle does not have nearly the impact on the OEC as decreasing the acquisition cost. Therefore, any design decisions that ultimately contribute to lowering the acquisition cost (i.e. reducing the empty weight of the vehicle or the installed horsepower) will improve the overall value of the design and should weight more critical. The relative impact of Acquisition Cost and Cruise Speed on the OEC can clearly be seen in Figure 12 and Figure 13 below across the applicable range of values generated by our tandem synthesis model for the pure tandem.

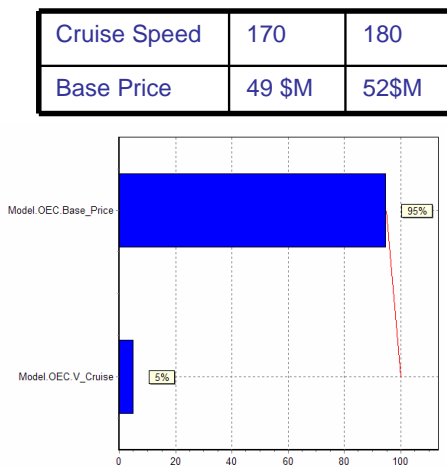


Figure 12: Acquisition Cost, Cruise Speed (OEC)

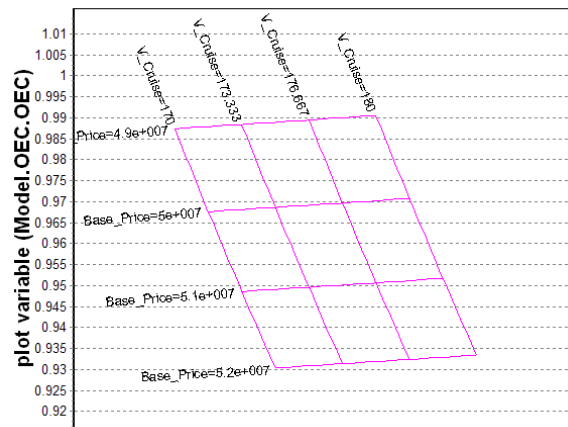


Figure 13: AC, Cruise Speed (OEC) II

The end-state of our sizing and synthesis to this point was the selection of a pure tandem rotorcraft that provided the best solution for a problem that we justified both from the customer and with analysis of the OEC (and cost model). Because we had progressed from an initial concept selection of the tandem family to a pure tandem design, we were ready to begin preliminary design of our actual rotorcraft called the Georgia Tech Tandem (GTT). Preliminary design results of the GTT and various design methods are presented in the following chapters.

4 Performance

The final specifications of the GTT are summarized in Table 4. Selection of these design parameters is the result of further iteration in the preliminary design—beyond concept selection—of our pure tandem configuration.

TABLE 4: GEORGIA TECH TANDEM AERODYNAMIC DATA

Unless specified different, all data is for ambient air at 3000 ft, ISA +20°C.

Gross Weight, lbs	105,334	Radius, ft	45.55
A_{eff} , ft ²	11,504	Rotor Shaft Separation, ft	59,215
Disk Loading, lbs/ft ²	9.2	Chord _{r/R=0} , in	52.66
Blade Loading, lbs/ft ²	99.5	Chord _{r/R=1} , in	26.33
Solidity	0.092	Best Endurance Speed, kn	115
CT/sigma	0.1	Cruise Speed, kn	168
CT	0.009	Cruise Adv. Ratio	0.4
V_{Tip} , ft/sec	700	Flat Plate Drag Area, ft ²	74.08
Required HP		Hover Performance	
Hover	13,790	FM_{max}	0.83
Max Endurance	7,840	$FM_{\text{FMR corrected}}$	0.73
Best Range	9,670	Maneuver	
Cruise	9,530	6°/sec Turn Load Factor	1.4
Tip Mach Number		6°/sec Turn Radius, ft	2679.8
M_{Tip} Hover	0.61	Autorotation	
M_{Tip} Cruise adv. Side	0.86	$t_{\text{equivalent [2]}}$, sec	1.9
M_{Tip} Cruise retr. Side	0.37	Auto Index AI [3]	15

All Engines Operating	MCP	IRP	MRP	CRP
HP _{Available Hover}	14,030	17,190	18,530	19,490
Hover Ceiling ISA, ft	10,400	14,000	15,100	15,800
Hover Ceiling ISA +20°C, ft	3,700	10,100	11,900	13,000
Max. R/C, fpm	1940	2928	3350	3649
Power Limited V_{max} , kts	215	235	242	246
One Engine Inoperative	MCP	IRP	MRP	CRP
HP _{Available Hover}	10,530	12,890	13,900	14,620

4.1 Drag Buildup

The equivalent flat plate drag area of the GTT was estimated by calculating the wetted area of each component using a method introduced in reference [2]. The method was written in a computer code and then validated using CH-47D data [4]. Table 5 shows the resulting drag comparison of the validation case, and Table 6 summarizes the flat plate drag components of the GTT.

The resulting total flat plate drag area was compared with historical data (Figure 14) that represented drag loading [4] as a function of gross weight. Because the GTT drag loading lies on an extended line of the average

design drag, the estimated drag is assumed reasonable with even a possibility to reduce drag using improved technology in further design iterations.

TABLE 5: DRAG ESTIMATION METHOD VALIDATION

Components	CH-47D [4] (GW: 33000 lbs)	Estimated Drag
Fuselage and engine nacelles	16.1	15.1
Rotor hubs	14.1	12.34
Landing gear	7.9	7.91
Miscellaneous	5.1	9.09 (including rotor pylon & fairing)
Total, ft ²	43.2	44.45

TABLE 6: FLAT PLATE DRAG AREA ESTIMATION OF GTT (GW:105,334 LBS)

Components	Estimated Drag	Components	Estimated Drag
Fuselage	22.97	Landing Gear (retractable)	0.0
Engine nacelles	12.6	IR Suppressors	2.0
Rotor pylon & fairing	7.73	Radar and missile warning equipment	0.6
Rotor hubs	26.8	Miscellaneous	1.36
Total, ft ²			74.08

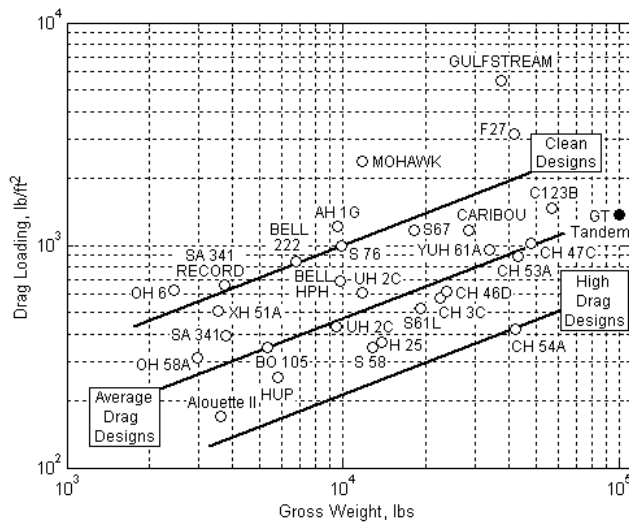


FIGURE 14: DRAG LOADING OF GTT WITH HISTORICAL DATA [4]

4.2 Performance Analysis

Figure 15 summarizes the power requirements of the GTT as function of forward flight speed. Mission cruise speed refers to the highest forward speed at which specific range is 99% of maximum [7]. Note that the GTT sizing was based on a one-engine-out (OEI) hover requirement at 60% fuel with the selected assumption that emergency

power is used at SL, ISA +20°C. The emergency power setting corresponds to a 10min rating for use. The required power shown here corresponds to a maximum TOGW, i.e., full fuel tanks.

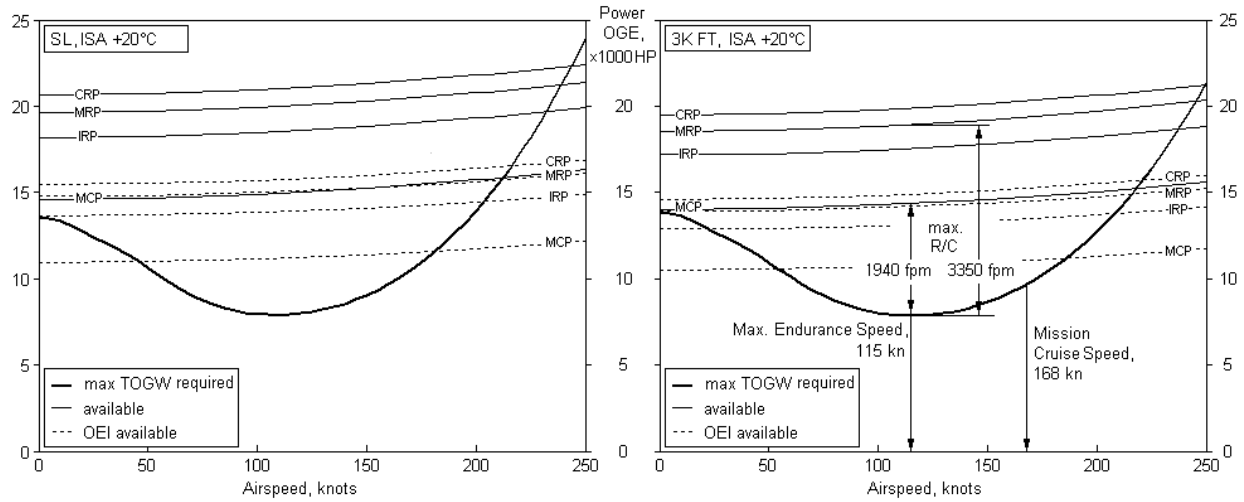


FIGURE 15: POWER REQUIREMENTS

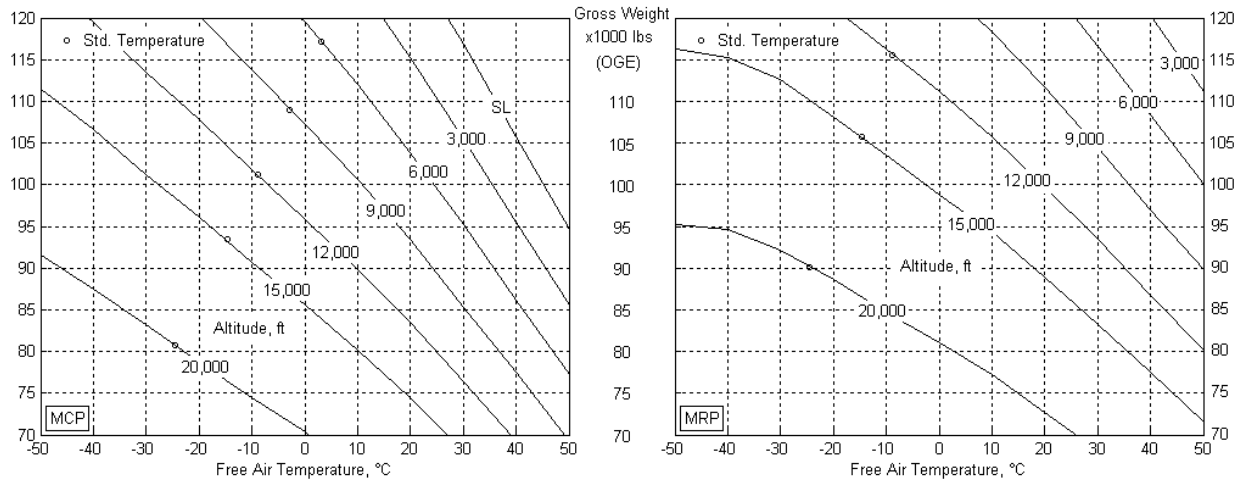


FIGURE 16: HOVER CEILING

Figure 16, Figure 17, and the cruise chart in Figure 18 were created in the style typically found in a pilot's operator manuals, such as those found in reference [3]. However, these charts are usually based on actual flight test data. The Hover Chart in Figure 17 illustrates the determination of the required torque to hover at max TOGW and the atmospheric conditions as specified in the RFP. Similarly, the Cruise Chart in Figure 18 provides a means of determining the required torque in forward flight.

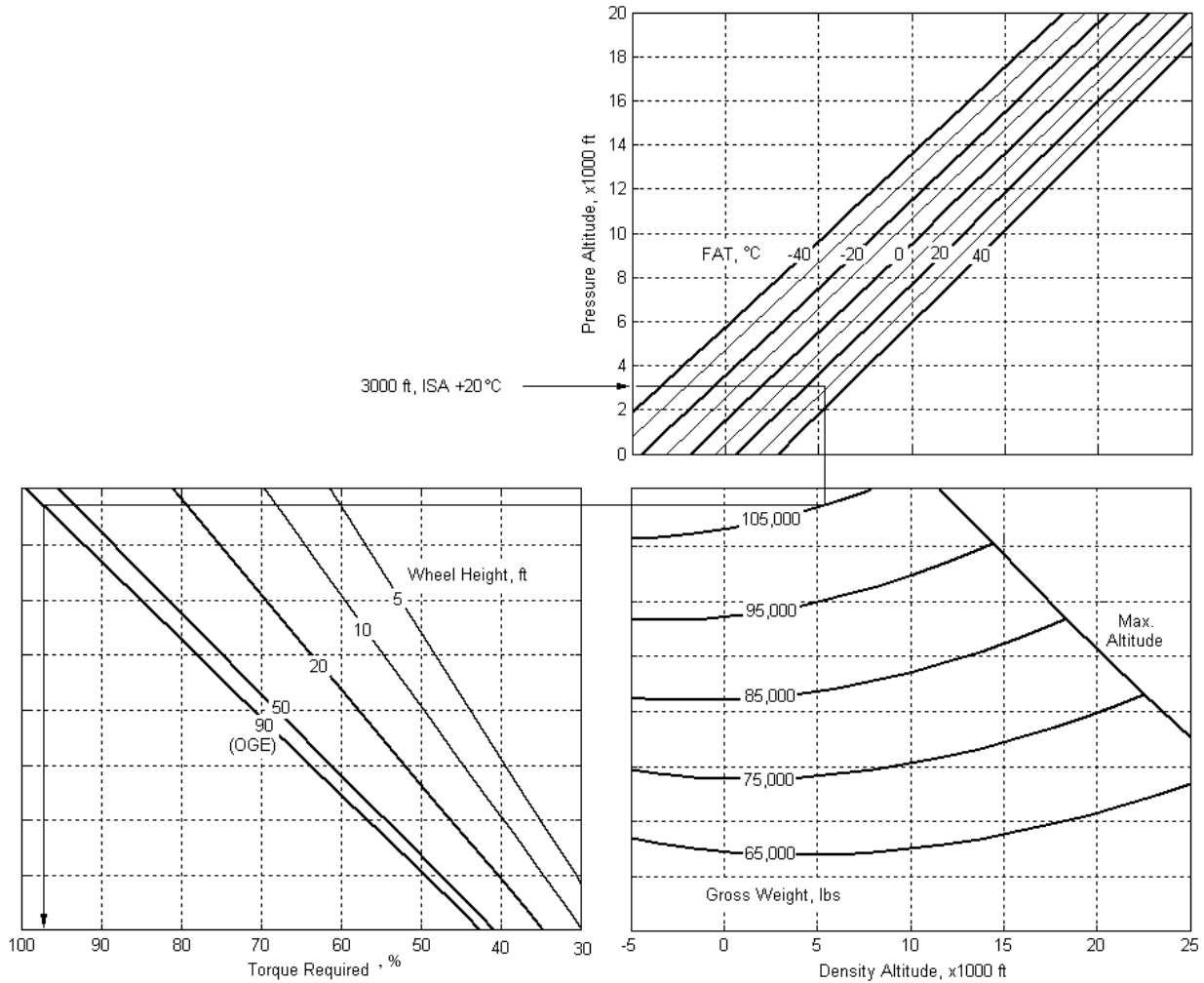
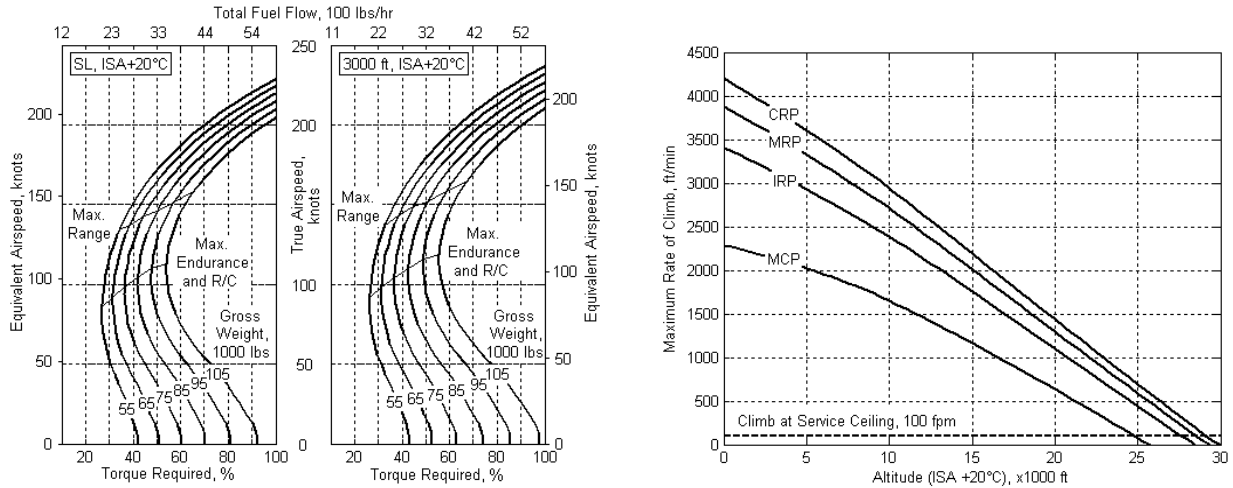
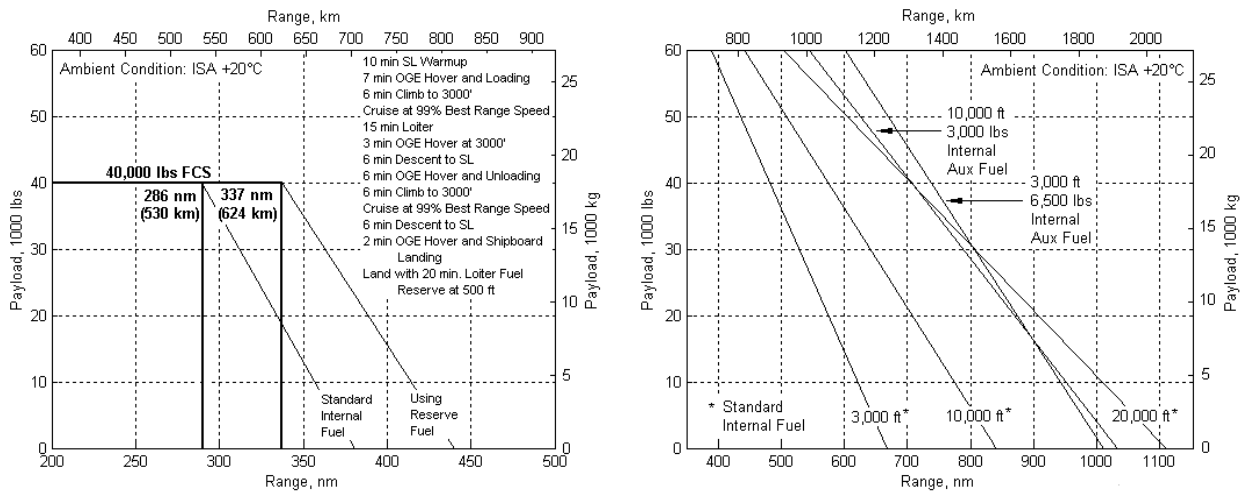


FIGURE 17: HOVER CHART

The cruise range of the GTT presented in Figure 19 corresponds to the cruise segments of the RFP mission profile. The available fuel for these plots is a result of the total internal fuel available minus the fuel consumed in mission segments other than cruise. Figure 19 shows that the GTT is capable of performing the required missions. In the instance of a mission abort at the landing zone, it is critical that the GTT be able to return to the L-class while still carrying the FCS. Hence, the return segment of the cruise range diagram accounts for a gross weight reduction from fuel consumption, only. Depending on altitude, auxiliary internal fuel tanks are required to complete the self-deployment mission of 1000 nm.



Left: Cruise Chart Right: Maximum Rate of Climb
 FIGURE 18: FORWARD FLIGHT PERFORMANCE



Left: Mission Cruise Range Right: Generic Payload-Range Diagram (Depending on Altitude and Internal Aux. Fuel)
 FIGURE 19: PAYLOAD-RANGE DIAGRAM

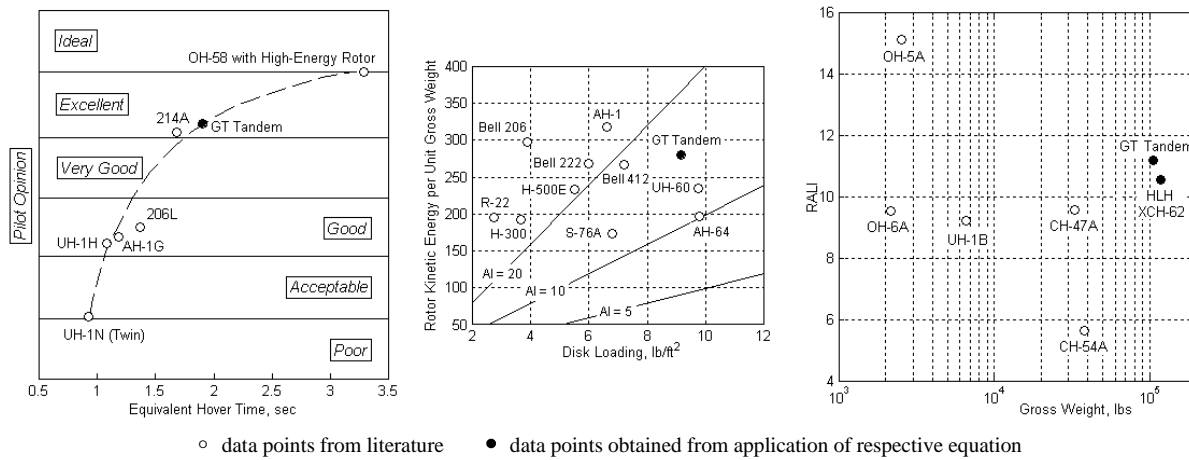
4.3 Autorotation

The capability of a helicopter to effect a safe landing in the event of complete power failure is typically determined by the establishment of an Autorotation Index (AI). While various definitions of AI's are found in literature, essentially they all represent a ratio of energy stored in the rotor to required power/gross weight. It is important to note that actual flight tests are the only solid proof of autorotation. Thus, Figure 20 contains a selection of AI's showing the GTT in comparison to already existing designs and demonstrating its autorotational capability.

While MIL-H-8501 specifies a maximum touchdown speed of 15kts, the establishment of that value lacks in actual test data [4]. However, at certain combinations of altitude and forward speed, the touchdown speed at the end

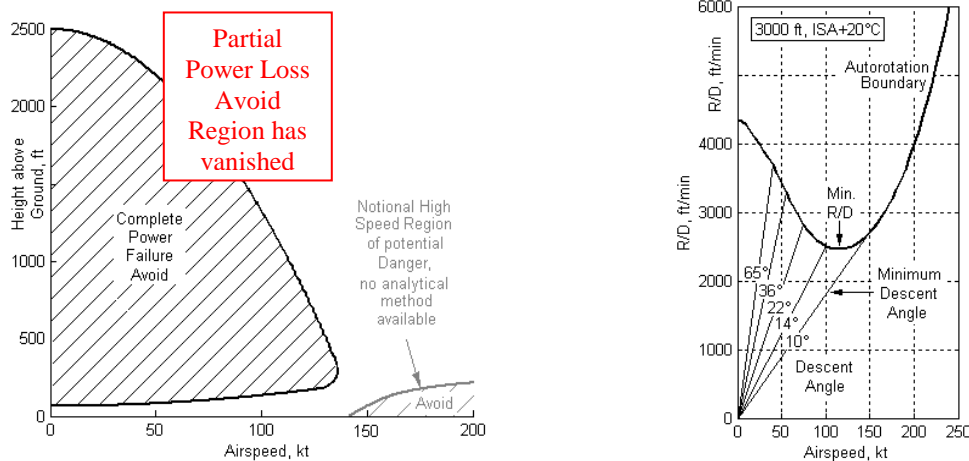
of the flare maneuver for autorotation will exceed the design capabilities of the landing gear. A first approximation¹ of the so called “*Deadman’s Curve*” for the GTT using a military pilot time delay of 2 seconds is shown in Figure 21. The actual avoid region for the GTT denoting partial power loss has vanished because of the installation of four engines [5].

An immediate interest of the pilot in an autorotating aircraft is finding a safe landing spot that is within the capable glide distance. The maximum glide distance of the aircraft, assuming a zoom maneuver is not possible, is a direct function of initial altitude and descent speed/angle (Figure 21). Please note that the underlying equation for R/D is subject to an inaccuracy margin of $\pm 15\%$ [7].



Left: Remaining hover time following complete power failure (power supplied by rotor kinetic energy) [4] Middle: Autorotation Index used by Sikorsky [5] Right: Relative Autorotational Landing Index [6]

FIGURE 20: AUTOROTATION INDICES



Left: Height-velocity diagram Right: Rate of descent in autorotation

FIGURE 21: AUTOROTATION LANDING CHARACTERISTICS

¹ The height-velocity curve of a helicopter is depending on characteristics that can accurately be determined in flight tests, only.

5 Rotor Design

To begin further preliminary design of the GTT we placed special emphasis on the main rotor and hub. Design of the main rotor system includes selection of the hub configuration, number of rotor blades, rotor disk diameter, tip speed, solidity, blade twist and taper, airfoil section design, planform area, and the selection of appropriate materials. A detailed design of the main rotor system for our proposed Heavy Lift VTOL design follows, and Table 4 presents a summary of the various aerodynamic parameters selected.

The main rotor is the most important part of designing a new rotorcraft. The selection of main-rotor parameters will dictate (or constrain) other characteristics of the rotorcraft as a whole e.g. maximum gross weight and physical size of the helicopter. Engineers take special care to select and vary parameters that provide the best balance between hover performance, forward flight performance, lowest cost, lowest weight, least amount of noise, lowest vibration, etc. The process is greatly complicated by the fact that these goals are often contradictory in nature. The selection of the GTT rotor parameters (Table 4) resulted from the detailed configuration trade studies, where the mission profile, RF method, and OEC directed the selection of design parameters in our Tandem model.

5.1 Rotor Diameter

Hover and autorotation greatly benefit from a large rotor diameter, but a small rotor minimizes cost and weight. Additionally, the RFP restricts size due to elevator constraints. For the GTT, the rotor dimensions are particularly crucial with considerations that include blade overlap and interference. The resultant disc loading of the GTT minimizes ground erosion and allows ground personal to perform cargo operations beneath the hovering helicopter.

5.2 Tip Speed

As for all relevant parameters, tip speed calls for contradictory requirements in hover and forward flight. Ultimately, it was chosen to provide both a good retreating and advancing blade flow environment. Additional effort went into considerations regarding a low rotor weight and a low noise level², which compete for high and low tip speeds, respectively. Due to the relatively high cruise speed of the GTT, particular attention was given to the advance ratio, such that the dimension of the reverse flow region is minimized and excessive blade stall on the retreating side is avoided without negligence of compressibility effects on the advancing side.

5.3 Blade Area

Blade area should be small for good hover performance, low blade weight, and low cost. Good maneuverability at high speeds, on the other hand, requires a large blade area. For the GTT, a 4-blade configuration was chosen to accommodate the heavy lift mission, to facilitate rotor blade intermeshing, and to minimize in-flight vibrations. The high cruise speed of the GTT particularly calls for an increased blade area because it lowers the mean blade lift coefficient, which in turn allows higher advance ratios [8]. Note also that a higher chord corresponds to an increased Reynolds number, resulting in slightly lower drag and higher maximum lift coefficients.

5.4 Solidity

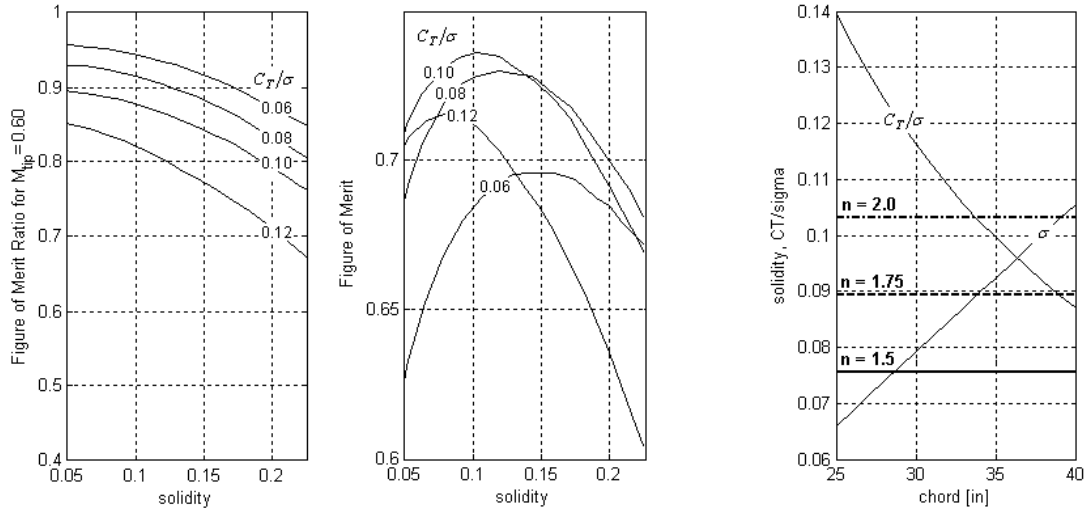
Solidity is determined by either hover performance or maneuver capability. To specify, the solidity corresponding to both requirements must be established and the higher value is implemented.

The solidity boundary in hover corresponds to minimum power requirements, hence to a maximum Figure of Merit (FM). FM, accounting for tip losses and profile drag, is essentially a function of the blade loading coefficient. An even more realistic FM can be found by applying the Figure of Merit Ratio (FMR). The latter method is based on empirical test data correcting for tip Mach number, root cutout, and other practical considerations. Since no test data specifically tailored for the GTT is available, the results of isolated rotor whirl stand tests representing a linear blade twist of -8° and a 20% root cut-out provided in reference [7] were used to reveal qualitative trends in FM. Figure 22 shows that a blade loading coefficient of 0.10 will maximize FM over the range of solidity values of interest.

The solidity boundary in forward flight imposes the avoidance of retreating blade stall. The maneuver capability is directly related to the load factor n [7,8], which is defined as the ratio of rotor thrust to gross weight and thus, is a function of speed and turn rate [4]. For the GTT, a sustained turn rate of $6^\circ/\text{second}$ (twice standard rate) at cruise speed will result in a load factor of 1.4. In an attempt to optimize the GTT, the load factor for the solidity maneuver requirement was set to 1.75 (Figure 22).

In comparing the solidities from both boundaries, the hover requirement was dominant. Final values for the GTT are listed in Table 4.

² Typically, tip speeds of 500 feet-per-second (fps) are considered quiet while tip speeds in excess of 750 fps are unacceptably loud [4].



Left: Hover Requirements in Terms of Figure of Merit Ratio [7] and Figure of Merit Right: Maneuver Requirements

FIGURE 22: SOLIDITY BOUNDARIES

5.5 Blade Twist and Taper

Blade twist improves the Figure of Merit in hover by reducing the induced power. However, high twist causes blade vibration in forward flight [5,9]. Once again, a compromise is required between hover and forward flight. A trade study was performed comparing various twist angles to determine the optimal blade twist. We limited our study to the consideration of linear twist to simplify the manufacturing process/cost.

Using simplified rotor trim equations [9], the lift distribution along the blade was calculated at four different azimuth angles using the VR7 airfoil as a baseline in Figure 23. Table 7 compares the dimensionless mean blade lift for one revolution of a blade in cruise and the figure of merit in hover for differing taper ratios. FM was calculated using combined blade element and momentum theory in hover [9].

It is obvious that higher twist angle in hover yields a higher figure of merit. However, since the GTT operates in cruise condition most of time, cruise performance was more likely considered. From Figure 23 and Table 7, the lower twist angle is more desirable for more uniform lift distribution at the advancing side, which produces lower vibration, and for higher mean lift, which is better for maneuver capability. Thus, the twist angle of -8° that shows moderate hover FM was selected.

In addition to twist angle, blade taper was introduced to yield a higher figure of merit without significant forward flight performance degradation. Too high a taper ratio causes higher profile drag that is associated with operating at small tip chord Reynolds numbers [5]. Also from a manufacturing viewpoint, lower taper ratio reduces

manufacturing cost. As a result, a taper ratio of 2, which has FM of 0.74 with -8 deg twist angle, was selected for the GTT.

TABLE 7: TRADE STUDY FOR TWIST ANGLE AND TAPER RATIO.

θ_{tw} , deg	-6	-8	-10	-12	-14
DBL	0.02097	0.02050	0.02002	0.01954	0.01906
FM (TR = 1)	0.703	0.712	0.721	0.729	0.737
FM (TR = 2: $c_{l/R=0} = 52.66$ in, $c_{l/R=1} = 26.33$ in)	0.732	0.739	0.747	0.753	0.759
FM (TR = 3)	0.748	0.755	0.760	0.766	0.770

$$\text{Dimensionless mean blade lift } DBL = \frac{L'}{\rho a c (\Omega R)^2}, \text{ Taper Ratio } TR = \frac{c_{Root}}{c_{Tip}}$$

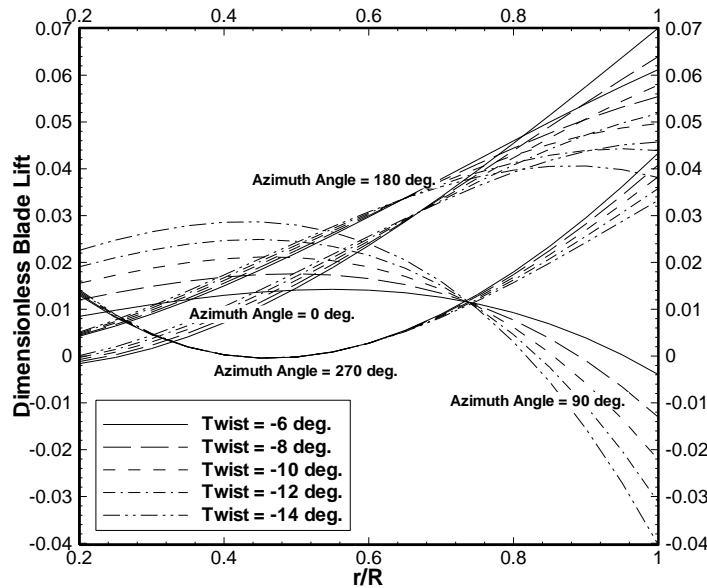


FIGURE 23: DIMENSIONLESS BLADE LIFT ALONG THE BLADE RADIAL DIRECTION FOR DIFFERENT TWIST ANGLE

5.6 Airfoil Design

In general, a high maximum lift coefficient is desired to delay retreating blade stall and a high critical Mach number is required to delay the onset of drag divergence for the advancing blade tip. A good lift-to-drag ratio over a wide range of Mach number is also required to reduce rotor profile power consumption. Zero pitching moment of the blade is preferred to avoid a cyclic variation in control force and resulting stick vibration [5]. These requirements are conflicting in the design of an airfoil because of the different local Mach number and angle of attack seen by an

airfoil at different radial and azimuth location during revolution. A compromise was required to produce the best performance over entire disk area.

Because the GTT carries 40,000 lbs of payload in a faster flight speed (168 knots) than a typical helicopter, both the hover and cruise condition airfoil performance must be maximized to fulfill hover and cruise requirements with minimum power consumption. Using only one airfoil for the entire blade while meeting all contradictory requirements significantly limits performance. Using too many airfoils causes manufacturing difficulties and possibly unintended performance degradation from the transition region. Thus, it was decided to use 4 different airfoils. A thick airfoil was located near the root for retreating blade stall then a best lift-to-drag ratio airfoil was used for the blade middle section, and finally a thin airfoil reduced advancing side compressibility effects at the tip. The V43015/V43012 airfoil has been selected for use between the root cut-out and 50% of the blade radius because of its high maximum lift coefficient at low Mach number. The airfoils for the middle and tip sections—the most important regions of a blade—were designed for the GTT to have the best performance for both the hover and high speed cruise condition.

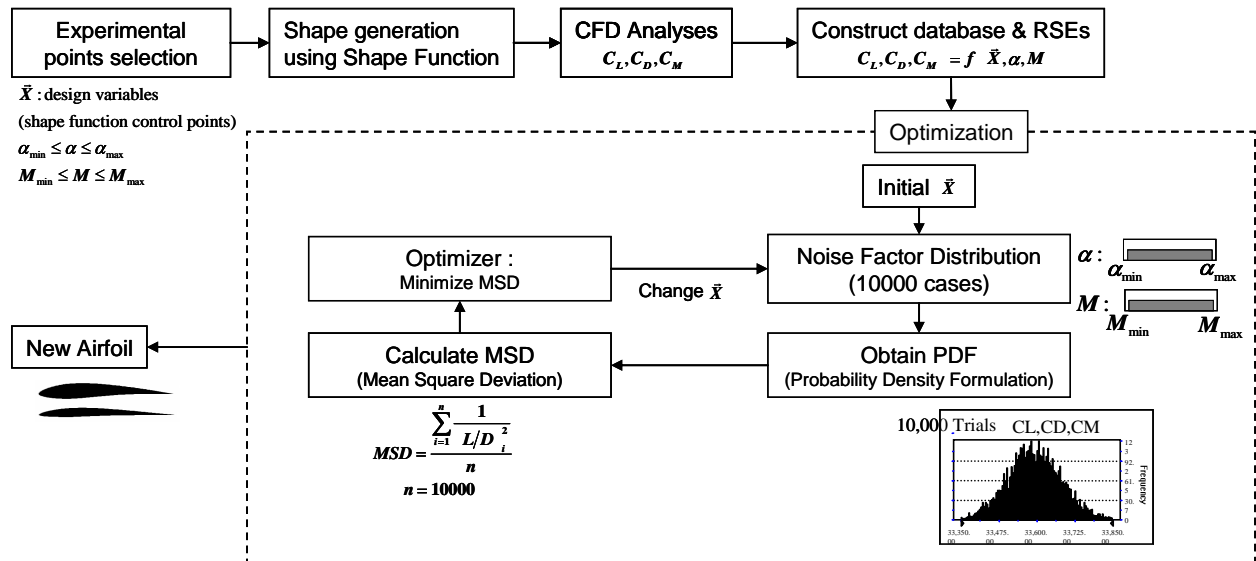
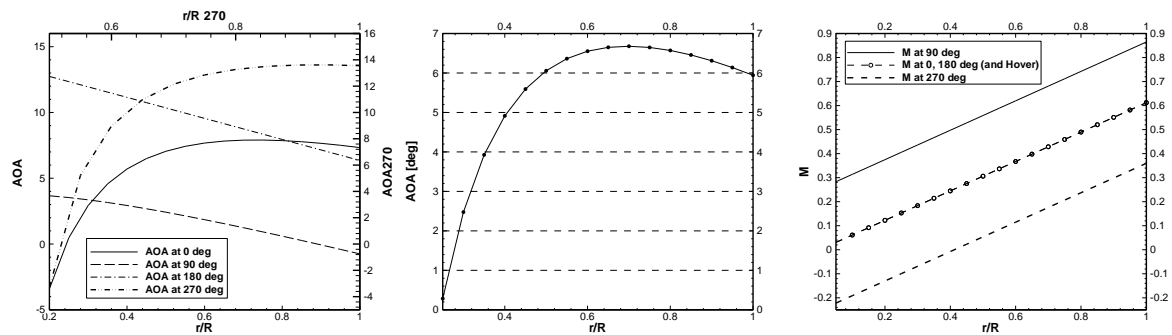


FIGURE 24: ROBUST DESIGN PROCEDURE FOR ROTORCRAFT AIRFOIL

For the design of these airfoil sections, a robust design method introduced in reference [10] was implemented to design a new airfoil, having the best performance over various operating conditions. The angle of attack, Mach number, and corresponding Reynolds number were noise factors representing different operating environments. The

control points of shape functions were selected as design variables. A cubic spline curve with four control points was used to represent the mean chamber line and a NURBS (Non-Uniform Rational B-Spline) curve was used to represent thickness distribution along the chord line. The robust design procedure for the GTT airfoil is shown in Figure 24.

To determine the range of angle of attack and Mach number, a simple rotor trim equation [9] was employed using VR7 airfoil data as a baseline with prescribed twist angle. Figure 25 shows the angle of attack and local Mach number distributions in the radial direction at different azimuth angles in both cruise and hover condition. Because it is difficult to predict airfoil performance using a numerical method in the high angles of attack of the retreating side, ranges of angle of attack and Mach number have been selected to include the entire hover regime as well as the advancing blade environment in cruise. The outboard section, after 80% of the radius, was designed so that the advancing side could delay the onset of compressibility effects. Table 8 summarizes the selected range of angle of attack and local Mach number for the new airfoil designs.



Left: Angle of attack distribution in cruise Middle: Angle of attack distribution in hover Right: Local Mach number distribution

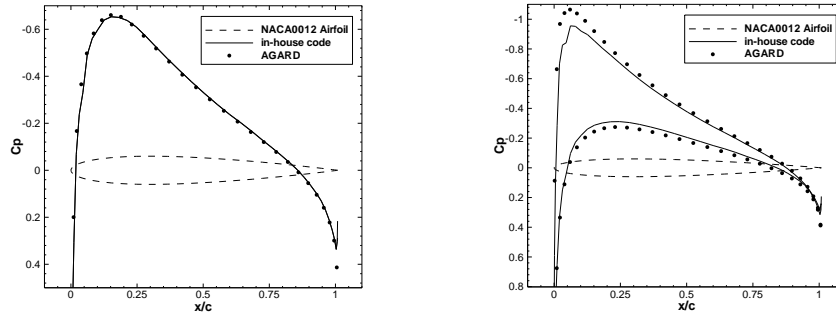
FIGURE 25: ANGLE OF ATTACK AND LOCAL MACH NUMBER DISTRIBUTION

TABLE 8: RANGE OF ANGLE OF ATTACK AND MACH NUMBER FOR NEW AIRFOIL DESIGN

Radial Range	α_{\min} , deg	α_{\max} , deg	M_{\min}	M_{\max}
$0.5 \leq r/R \leq 0.8$	0.27	10.0	0.3	0.8
$0.8 \leq r/R \leq 1.0$	-1.00	1.0	0.7	0.9

A database was constructed by analyzing various shapes of determined airfoils based on DoEs in various flow conditions using in-house Navier-Stokes CFD code. Program XFOIL [11], a high-order panel method with the fully coupled viscous/inviscid interaction method, was used to predict the new design airfoil performance at subsonic to save analysis time. Figure 26 shows the validation case of in-house CFD code with NACA0012 airfoil experimental

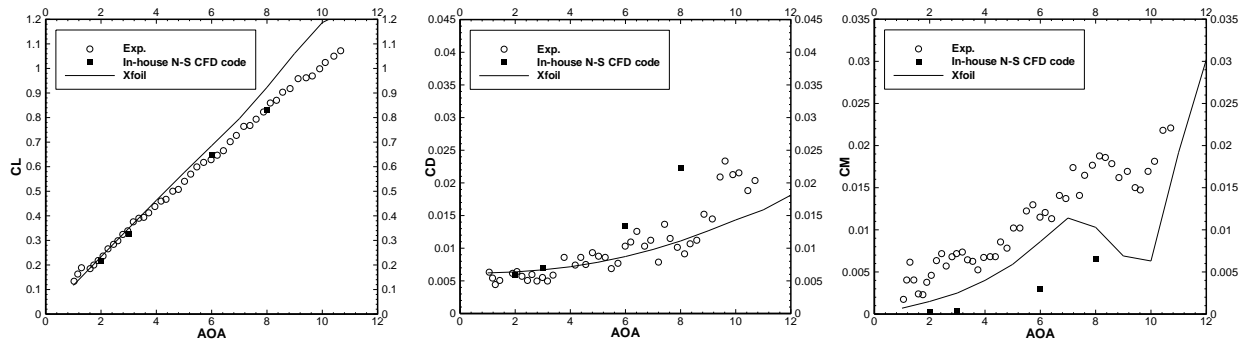
pressure coefficient data from AGARD. Figure 27 shows the validation case of XFOIL and in-house code with NACA0015 experimental data. New airfoils - GTHLH1 and GTHLH3 - were designed, following the procedure shown in Figure 24. Shape and implementation are shown in Figure 28 and Figure 33, respectively.



Left: Mach 0.71, Angle of attack = 0°

Right: Mach 0.63, Angle of attack = 2°

FIGURE 26: IN-HOUSE CFD CODE VALIDATION WITH NACA0012 EXPERIMENTAL DATA FROM AGARD



Left: Lift coefficient comparison

Middle: Drag coefficient comparison

Right: Moment coefficient comparison

FIGURE 27: XFOIL AND IN-HOUSE CFD CODE VALIDATION WITH NACA0015 EXPERIMENTAL DATA (M=0.29, RE=1.59E6)

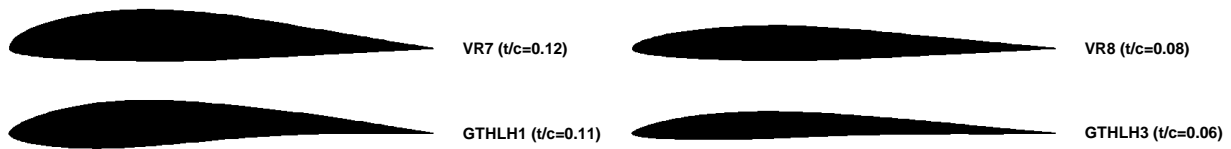


FIGURE 28: NEW AIRFOIL SHAPE, GTHLH1 ($0.5 \leq r/R \leq 0.8$), GTHLH3 ($0.8 \leq r/R \leq 1.0$)

Figure 29 and Figure 30 show the comparison along the radial direction between the baseline airfoil and new airfoil in hover and the advancing side of the GTT cruise condition. Both VR7 and GTHLH1 have similar

performance in the hover condition and possess a similar FOM. On the advancing side, GTHLH1 and GTHLH3 have better lift and drag characteristics than the baseline airfoils. However, the pitching down moment of new airfoils was higher than baseline airfoils, so a trailing edge tab is suggested to suppress the pitching moment. Figure 31 shows the shock structure formed on the VR8 and GTHLH3 airfoil at the advancing side tip. Although the shock on the GTHLH3 is weaker than VR8, especially on the lower surface, the blade is still operating above the drag divergence Mach number. Therefore, a swept blade tip was introduced to delay compressibility effects. A swept tip can also help to suppress the pitching down moment at the tip, which is required for new airfoil, because of a downward load acting behind the structural axis and twisting the blade nose up [4]. The lift coefficients of GTHLH1 and GTHLH3 for various Mach number and angle of attack are plotted in Figure 32 for design reference.

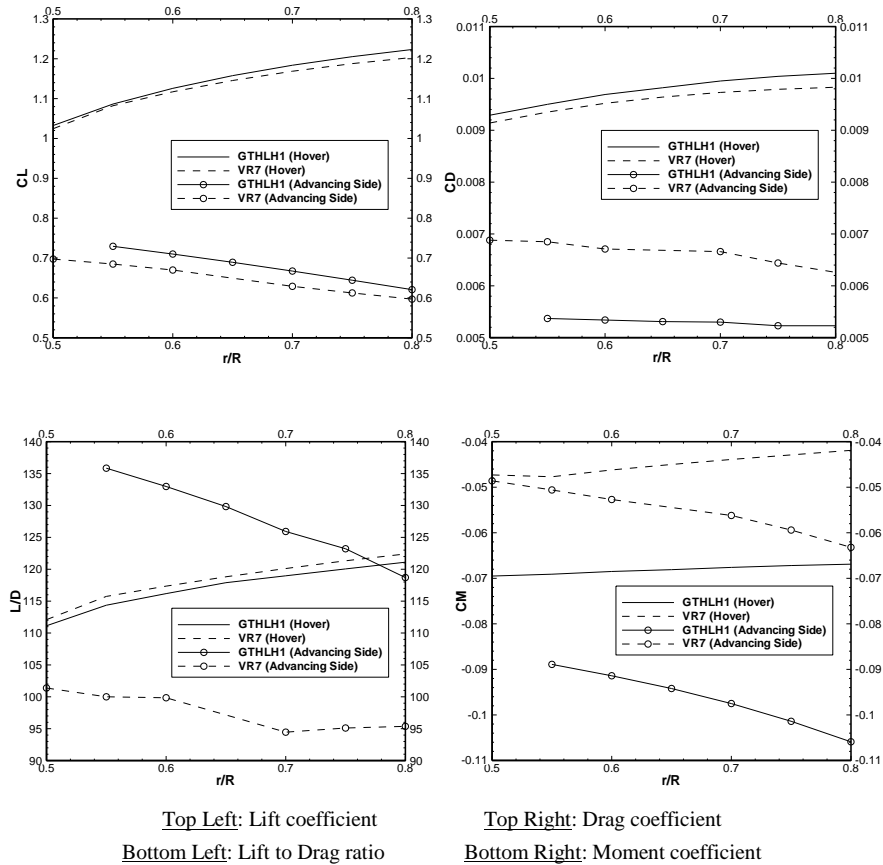


FIGURE 29: VR7 AND GTHLH1 PERFORMANCE (XFOIL SOLUTION)

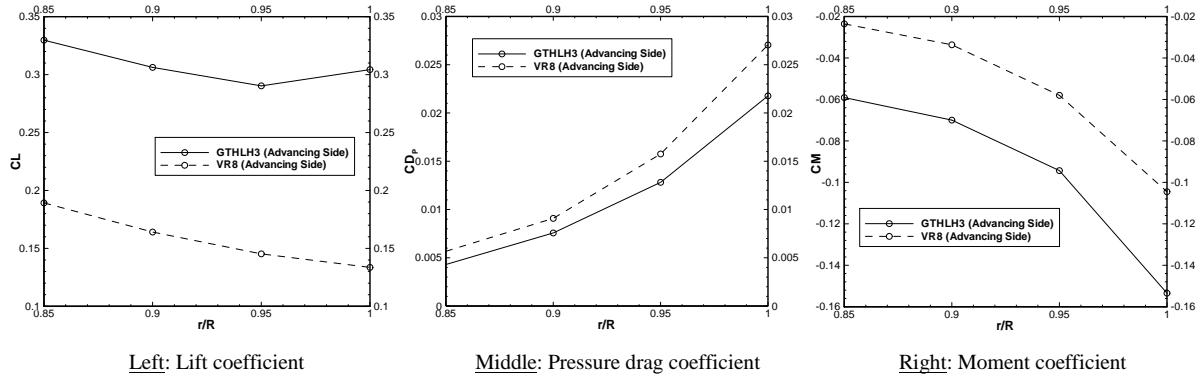
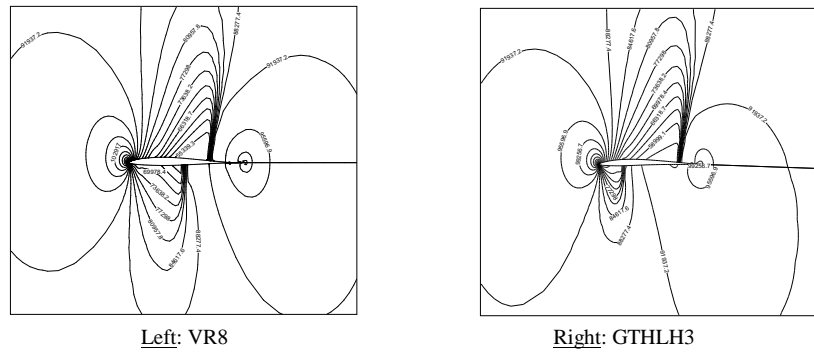


FIGURE 30: VR8 AND GTHLH3 PERFORMANCE IN ADVANCING SIDE (IN-HOUSE CODE EULER SOLUTION)



(Euler solution from in-house code)

FIGURE 31: PRESSURE CONTOURS AT THE ADVANCING BLADE TIP

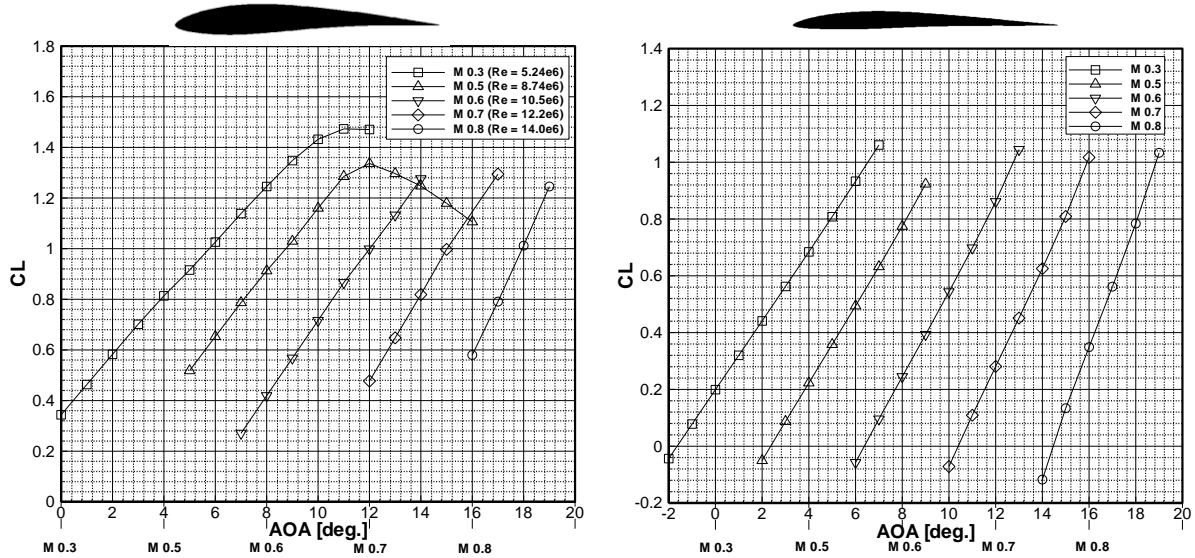


FIGURE 32: NEW AIRFOIL LIFT COEFFICIENTS

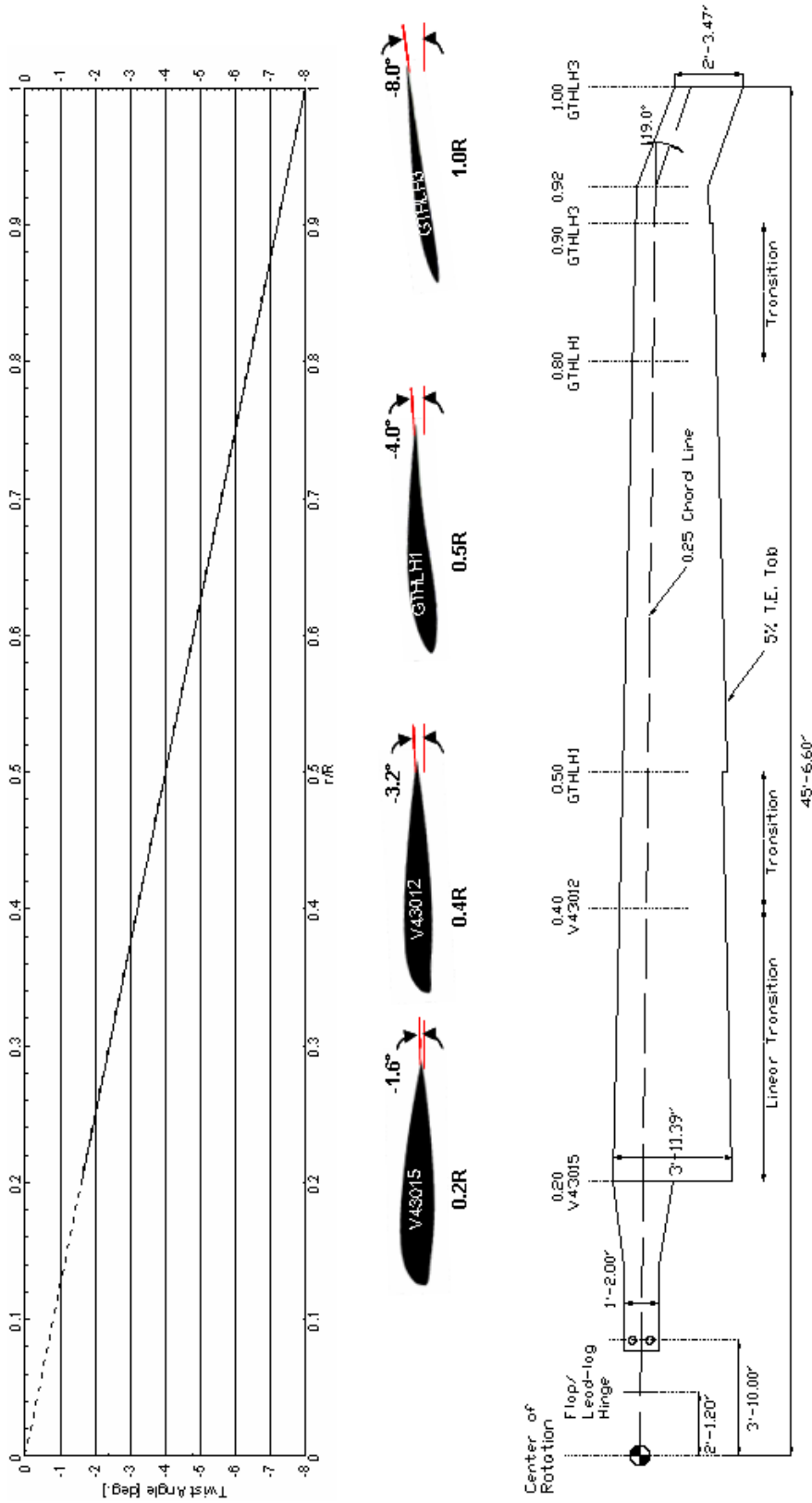
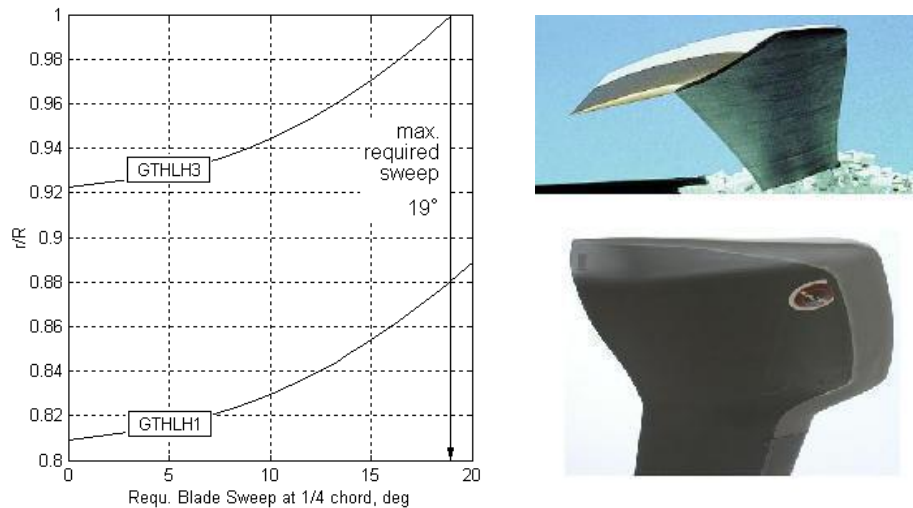


FIGURE 33: GTT ROTOR BLADE DETAILS

5.7 Blade Tip Design

While simple, square blade tips have the advantage of being the least expensive, the GTT blade tips required sweep to alleviate compressibility effects and noise on the advancing blade. Additionally, sweep introduces a favorable dynamic twist that helps reduce Mach tuck³. Reference [5] provides a concise introduction in swept tips and their aerodynamic advantages. The GTT blade tips incorporate taper and a constant sweepback angle. The latter is applied at $\frac{1}{4}$ chord. In order to avoid inertially coupled blade dynamics by too aft a center of gravity (C.G.), sweep is typically kept below 20° [5]. The determination of the GTT tip sweep is shown in Figure 34. The actual implementation can be found in the detailed design drawing of the blade in Figure 33.



Left: Required Sweep depending on M_{dd} and Radial Location Upper Right: Blade Tip Anhedral of the Sikorsky S-92 Search and Rescue
Lower Right: BERP Rotor Tip of the EH101 Merlin (Italian Naval Aviation)

FIGURE 34: BLADE TIP DESIGN

Please note that an appropriate anhedral would further improve the aerodynamic performance of the GTT blade tip, as shown by the unique tip of the UH-60 Blackhawk and the Sikorsky S-92 (Figure 34). However, respective trades and analyses could not be performed.

Another unique tip design is the BERP rotor (Figure 34), a result of various innovations in both airfoil and tip shape design [5]. Despite of a significant portion of ongoing research still being devoted to tip vortices, the BERP rotor is delaying flow separation partly by taking advantage of vortex flows. Its practical implementation in a

³ Mach tuck is the tendency of airfoils to pitch nose down in supersonic flow regimes.

Westland Lynx in 1986 clearly demonstrated superior performance alleviations, especially at high speed forward flight. According to reference [12], this Westland Lynx “*currently holds the absolute straight-line speed record for a single-rotor helicopter at some 250-kts (400-km/hr; 287-mi/h)*”. Thus, the BERP rotor is strongly recommended as a potential candidate for the practical realization of the GTT.

5.8 Root Cut-Out

The inboard 15-30% of the rotor blade are of little aerodynamic use, only [9]. Additionally, the reverse flow region on the retreating side imposes not only an aerodynamic uselessness, but also a performance disutility of the respective blade region. However, the effect of the reverse flow region is said to be negligible for advance ratios smaller than 0.5 [9]. Thus, the inboard 20% of the blade inherently provide the necessary space for the mechanical arrangement of hinges and flexures without rigorous aerodynamic disprofit [13]. Accordingly, the root cut out for the GTT takes 20% of the rotor radius (Figure 33).

6 Hub Design

The design of the GTT rotor hub is critical to the overall design of the vehicle. The hub-type selection process and specifications are detailed in the following sections for the hub design. We recognized that optimization of the hub design depends on accurate prediction of loads while at the same time refining the design for minimum weight. The rotor hub drag is a significant contribution to overall drag the GTT, and it was desired that this parameter be minimized. Reducing the wetted area and streamlining the contours are critical to achieving this goal. In general, the hub design presented here presents the results of the concept selection trade study and recommendations for inclusion of advanced material technology.

6.1 Selection of Candidate Hub Systems

Several hub systems were considered during the initial GTT preliminary design phase. The candidate configurations as well as the major advantages and disadvantages are shown in Table 9. The fully articulated rotor was chosen as the preferred configuration for the design because of the RFP blade folding requirement and maturity of the technology. The fully articulated hub also provides the advantage that advanced technology can be incorporated in the design without requiring a complete redesign of the hub—an ideal option for our level of design.

TABLE 9: ROTOR HUB CANDIDATE CONFIGURATIONS

Rotor Type	Advantages	Disadvantages
Teetering	Simplicity Relatively Low Cost	Control Moments Only from Thrust
Hingeless	No Flap or Lag Hinges – Fewer Parts Lower Maintenance Required	Expensive Difficult to Design Blade Folding Alters Stiffness Large Bending Moments Transmitted to the Structure
Bearingless	Low Part Count Lower Maintenance Required	Difficult to Design Blade Folding Alters Stiffness Expensive
Full Articulated Rotor – Traditional Design	Proven, Mature Design and Technology Control Moments from Thrust Tilt and Hinge Offset	Complex High Number of Parts Maintenance Intensive
Fully Articulated Rotor with Elastomeric Bearings	Proven, Mature Configuration, Technology can be Infused for Upgrades Reduced Maintenance Control Moments from Thrust Tilt and Hinge Offset	Expensive Difficult to design

6.2 Hinge Offset and Power Blade Folding

Figure 35 is a “notional” depiction of the rotor hub system rendered in the 3-D modeling software package Catia[®]. The rotor hub is a fully articulated system with a hinge offset from the hub center to the flapping/lead-lag hinge of 2.1 feet, (4.6% of the rotor radius). Also depicted in Figure 35 is the blade folding scheme.

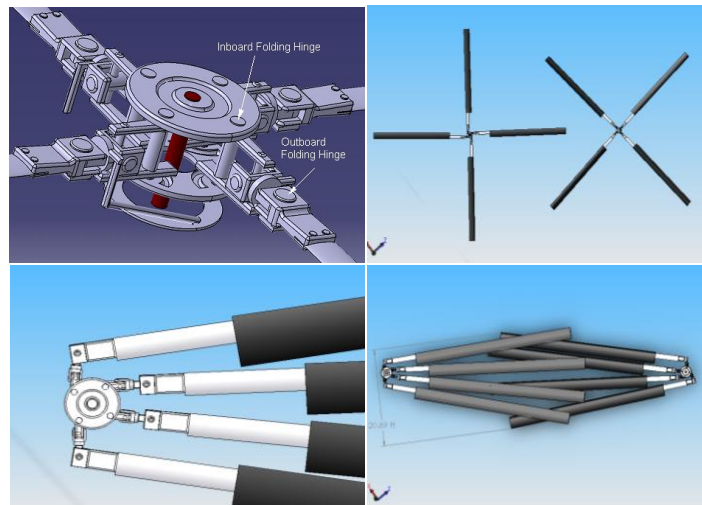


FIGURE 35: NOTIONAL GT ROTOR HUB CONFIGURATION

Blade folding is accomplished through a dual set of hinges on each blade—inboard and outboard hinges. The interior of the hub contains a hinge mechanism that allows each blade to be folded in a particular direction. The

mechanism is position-critical in that the rotors must be advanced to a particular position in order to activate the folding sequence. The mechanism provides safety interlocks to prevent in-flight malfunction, to prevent damage to the vehicle from improper sequencing, and to provide positive cues to the crew for safe flight conditions [8]. An electromechanical actuator housed within the outboard hinge of each blade controls the outer folding motion and an actuator on the underside of the hub controls the pivoting of the blade and control assembly. Both of these actuators are not depicted for clarity, and all of the dampers or springs for the hub are not shown.

6.3 Material Selection

The structural components of the rotor system require high strength, lightweight materials. High strength metallic alloys such as steel, aluminum, and titanium are required for the main shafts and inner supports of the GTT. Advancing material technology allows, however, for the inclusion of advanced materials, like elastomerics, in the hub design. Figure 36 shows a typical elastomeric bearing that can replace articulation hinges with a single elastomeric component. It does this because an elastomeric bearing is a mechanical structure comprised of alternating layers of rubber and metal laminates configured to accommodate various load and motion modes [14]. This unique bearing configuration results in various advantages listed in Table 10.



FIGURE 36: TYPICAL ELASTOMERIC SPHERICAL BEARING

TABLE 10: ADVANTAGES OF ELASTOMERIC COMPONENTS [14]

Advantages of Elastomeric Components
Reduction in number of parts
Reduced Rotor System Weight
Maintenance free
Reduce DOC and Maintenance Cost
Part replacement based on “on condition” visual inspection approach
Absence of rubbing, wearing or rolling of sliding/rolling elements
Elimination of seals, boots, or dust cover
Elimination of contamination by such environmental matter as dirt, dust, or water

6.4 Rotor Hub Weights and Parts Count

During initial sizing of our vehicle, weight equations estimated the total GTT rotor weight (including blades) to be 9070 lbf (9% of GW). Hub and blade retention were estimated to total 5260 lbf for both rotors, or 2630 lbf per rotor with each blade weighing 805 lbf. The published data in reference [15] provided weight and balance information on the Boeing Vertol Company heavy-lift prototype helicopter (HLH) which we used for validation of these estimates. The HLH report indicated that the rotor group (including blades) accounted for 11.0% of the GW of

the vehicle (134,000lbf), with each individual blade weighing 1,180 lbf. This implied an individual hub weight of 2650 lbf. From preliminary estimates, we expect infusion of advanced technology elastomers to reduce the hub weight by approximately 15% based on the Rotary Wing Structures Technology (RWST) program. The number of parts in a traditional fully articulated rotor could easily surpass one thousand. The inclusion of advanced technology materials, like elastomeric bearings, reduces the part count by an order of magnitude. As an example, an advanced design Low-Maintenance dry hub was described as containing approximately 120 parts [14].

6.5 Control Power Requirements

The GTT must have sufficient control power across the flight envelope for safe operation and ability to complete the mission. The GTT achieves maneuverability in each axis by combinations of rotor collective and cyclic control inputs. Pure vertical control is provided by collective input to both rotors. Differential collective provides longitudinal control, and lateral control is provided by coordinated cyclic inputs. Yaw control is accomplished with differential cyclic input. The GTT requires that the control system gains and mixing ratios from pilot input to the rotor hub be carefully designed to provide adequate authority throughout the flight envelope. Our efforts in fixing these mixing parameters were incomplete but yielded favorable initial results shown in the GTT's stability and control.

6.6 Control Power in Autorotation

During autorotation the handling qualities of the GTT are substantially altered. Reference [16] investigates the directional stability of the tandem helicopter using both flight and wind tunnel tests. In the document, pilots reported that lateral disturbances could produce large amplitude lateral oscillations during autorotation [16]. Because of this, the control power of the GTT must be sufficiently high to allow damping of oscillations in autorotation regardless of the status of stability augmentation systems. It is desired that the control power would also permit maneuvering to a desirable landing site. The trim data for the GTT—presented later—revealed that the control sensitivities are sufficient at hover and forward flight.

6.7 Precision Maneuvering/Cargo Handling

Sufficient control power from the hub design is also required to precisely hover, especially during GTT cargo loading and unloading. The "Position Hold" mode of the Control Augmentation System (CAS) or the adaptive neural network flight control system (FCS) provides for precise maneuvering while loading or unloading. A

distributed avionics integration design utilizing various radars, inertial navigation systems (INS), and GPS receivers are filtered using an Unscented Kalman Filter to provide necessary feedback. In the “Position Hold” mode, flight control trim selectors function as position incremental controls where “one momentary input” equates to a set position change increment. Alternatively, the “Position Hold” function can be used in “Relational” mode where the target position is not fixed in inertial space but is attached to the cargo. The “Position Hold” in this mode adjusts for the moving load conditions found during shipboard operations.

6.8 Rotor Dynamics and Vibration

The main rotors of the GTT are the primary source of vehicle vibration and natural modes of the aircraft. Therefore, it was essential that the dynamics of the rotors be investigated to refine the overall hub and blade design and reduce the potential damage from resonance. Additionally, analysis of the rotor dynamics can ensure passenger safety and comfort as well as vehicle fatigue and accuracy of flight control sensors. The software program Dymore[®] was utilized to investigate the GTT dynamics. Dymore[®] is a multi-body dynamics modeling tool developed by Olivier Bauchau at the Georgia Institute of Technology.

6.9 Single Blade Analysis

The main rotors of the GTT were designed for a rotational velocity of 147 RPM through aerodynamic requirements. It was important that the natural frequency of the blades did not coincide with this rotational speed. For the four bladed rotor, reference [7] indicates that 4/rev frequencies for out-of-plane motion and 3/rev and 5/rev frequencies for in-plane motion should especially be avoided. The frequency analysis was accomplished by modeling the GTT rotor blades in Dymore[®]. An assumption was made that the hub and shaft were rigidly supported. The results of the frequency analysis are shown in Figure 37. The fan plot provides the natural frequency of the blades as a function of the rotor angular velocity. The modes on the fan plot include the first in-plane mode, the first torsional mode, and the first three flap-wise modes. Reference [8] indicates that all modes through the eighth harmonic should be considered in order to avoid resonance, however, the higher harmonics were not included in Figure 37 because some of the higher harmonic data from the HLH report was not available for validation. Also, we believe that the most valid data is presented concisely in this figure. The analysis indicated that—while the rotors turn at the normal operating angular rate—the second flapping mode frequency is safely between the 4/rev and 5/rev frequencies, and the first lead-lag mode frequency is safely between the 3/rev and 4/rev frequencies. The first

torsional mode frequency is slightly higher than the 5/rev point. This could present a potential instability, however, the dynamic model was found to under-predict the torsional mode frequency at the operating RPM by about twenty percent. In that case the frequency separation would be even greater. The model otherwise provided results within about 5 percent of the HLH published data when validated against reference [15].

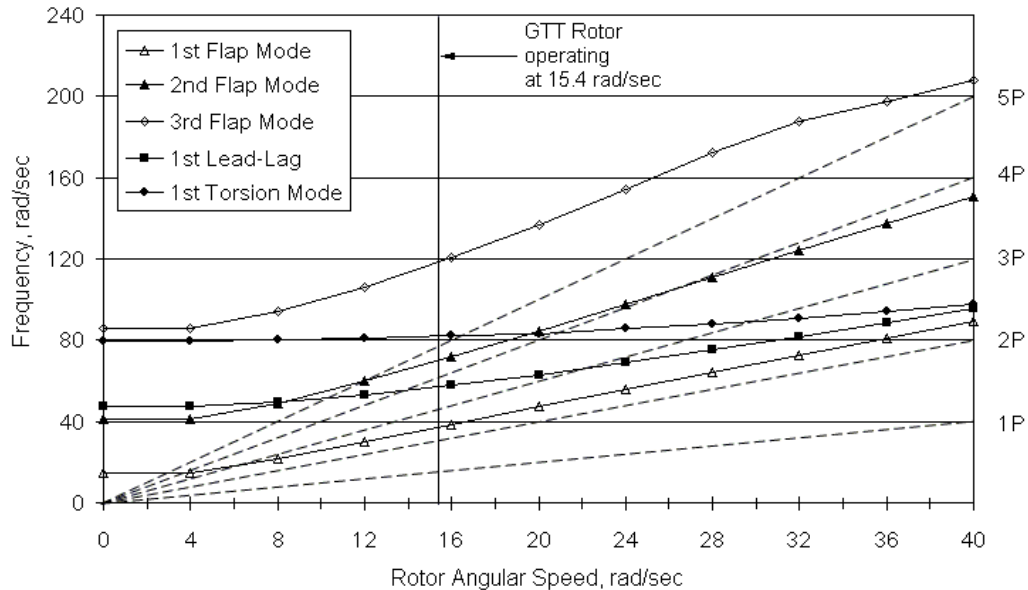


FIGURE 37: SINGLE BLADE ANALYSIS FAN PLOT

6.10 Ground and Air Resonance

Ground and air resonance are potential dangers and destructive conditions for the GTT. It is paramount that such threats do not develop in the GTT throughout its flight envelope and gross weight range. Ground resonance is a coupling of the lead-lag motion of the blades with the motion of the helicopter on its landing gear; this resonance can destroy the vehicle within seconds. In order to make a preliminary investigation of the ground resonance behavior, Dymore[®] was used again to create a model of the vehicle. It was then possible to visualize the ground resonance behavior analytically. The results indicated that dampers in the landing gear were required to provide the necessary damping that would suppress oscillations. Air resonance results from the interaction of the body pitching and rolling frequencies—determined from the rigid body dynamics—with the rotor in-plane frequencies. Damping that suppresses air resonance is provided by the lead-lag torsional dampers and both the aerodynamic and inertial damping of the rotors.

6.11 Additional Considerations

The absence of resonance for the GTT in the above analysis fails to totally ensure that the condition will not exist. More detailed analyses of the frequencies are required as the design progresses and should be coupled with a wind tunnel and prototype flight test program. Furthermore, the rotors are not the only source of vibration in this problem. The engines and drive train must also be considered. Finally, aero elastic effects such as rotor blade flutter and torsional divergence are to be considered for a thorough analysis of dynamics and vibration.

7 Structural Design

7.1 Structural Criteria

The GTT criteria for structural design were established with the RFP and Aeronautical Design Standards [17]. The RFP specified the normal load factor at the GTT design takeoff gross weight as $-0.5g$ to $+2.5g$ with the added ability to sustain a turn rate of 6 degrees per second in cruise speed. The GTT maneuvers for symmetrical and asymmetrical flight are listed in Table 11.

TABLE 11: SYMMETRICAL AND ASYMMETRICAL FLIGHT MANEUVERS [7]

Maneuver	Remarks
Hover	The load factor for hover is one
Takeoff and Climb	Depending on the type of takeoff maneuver, jump takeoff or standard takeoff, the load factor typically does not exceed 1.6 for takeoff and 1.5 for climb out.
Level Flight	The load factor for level flight is dependant on the force balance for trimmed flight and is a function of airspeed.
One-g Dive	The load factor for this maneuver is one
Pullup at Design Gross Weight	This maneuver demonstrated the maximum load factor attainable for symmetric flight.
Pushover	This maneuver results in a negative load factor
Rolling Pullup	The load factor for this maneuver is inversely proportional to the cosine of the bank angle.
Sideslip, Yaw, and Sideward Flight	These maneuvers generate the highest lateral load factors.

7.2 Geometry

The geometry of the GTT rotorcraft was generated from the Model Center© Tandem sizing tool mentioned earlier. A summary of the main geometric outputs from the results of this tool is shown in Table 12. 3 view drawings of GTT are presented in Section 12.

TABLE 12: GEORGIA TECH TANDEM GEOMETRY

Fuselage		Aft Section		Main Fuel Tank			
Length (ft)	72.2	Rampwell (ft)	7	Length (ft)	15.00		
Width (ft)	15	Length (ft)	15	Width (ft)	5		
Height (ft)	15	Rotor		Height (ft)	3		
Fwd Rotor Hub Height (ft)	17	Hub Spacing (ft)	59.22	Volume (Gal)	1683.11		
Aft Rotor Hub Height (ft)	23			Rotor Diameter (ft)	91.10	Reserve Fuel Tank	
Nose Section		Blade Thickness (%)		Length (ft)	4.89		
Cockpit (ft)	6			V43015	15	Width (ft)	4
Cabin (ft)	9			V43012	12	Height (ft)	2
Mid Section (Cargo Bay)		GTHLH1	11	Volume (Gal)	292.44		
Length (ft)	42.2	GTHLH3	6				
Width (ft)	11.9						
Height (ft)	10.5						

7.3 Materials

Materials of the GTT must be cautiously selected and attributed to minimize cost and facilitate manufacturability. They must ensure safe margins of strength and corrosion resistance. For such a selection, material characteristics were collected in Table 13.

TABLE 13: PUGH MATRIX OF CANDIDATE MATERIALS

Material	Weight	Specific Strength	Specific Stiffness	Temp Limit	Corrosion Resistance	Fatigue Resistance	Repairability	Machineability	Cost	Production Cost
Aluminum Alloy	0	0	0	--	-	0	++	+	++	-
Steel Alloy	++	0	0	++	0	++	0	0	++	-
Titanium Alloy	0	0	0	++	0	0	--	-	0	-
--E glass / Epoxy	--	+	-	--	++	++	++	++	++	--
S glass / Epoxy	--	++	-	--	++	++	++	++	0	--
Boron / Epoxy	--	++	++	--	++	++	++	++	--	-
Carbon / Epoxy	--	++	++	--	++	++	++	++	--	-
Boron / Al Alloy	0	0	++	0	-	0	0	--	--	+
Boron / Pl	--	++	++	0	++	++	0	0	--	-
Kevlar	--	++	0	--	++	++	++	++	0	-

After reviewing candidate materials, a more subtle selection can be made given different alloys in Table 14.

TABLE 14: ALUMINUM ALLOY COMPARISON

Name	2024-T4	2219-T62	6061-T6	7050-T7651	3003-O	6063-T6
Density (g/cc)	2.78	2.84	2.7	2.83	2.73	2.7
Hardness (Brinell)	120	115	95	147	28	73
Tensile Strength, ultimate (Mpa)	470	415	310	550	110	240
Tensile Strength, yield (Mpa)	325	290	275	490	40	215
Modulus (Gpa)	72.4	72	69	72	69	69
Machinability (%)	70		50	good	10	50
CTE (ppm/deg C)	23.2	22.3	23.6	23.6	23.2	23.4
Thermal Conductivity (W/m-K)	120	120	167	153	193	201
Notes	high strength, weldability	e-beam weld	common	very high strength, hard, weldable	extrusion, soft, nonheat-treatable	extrusion

Table 15 presents the materials selected for the GTT from these tables and vehicle load analysis.

TABLE 15: CONCEPT MATERIALS

Fuselage Frame	Al 6061-T6
Bulkheads	Al 6061-T6
Spar Caps	Al 6061-T6
Longeron	Al 6061-T6
Skin	Al 2024-T4
Doors	Al 2024-T4
Boxes	Al 2024-T4
Firewalls	Al 2024-T4
Rotor mast	S 21904 (Steel Alloy)
Rotor mast supporting structure	S 21904
Landing gear	Al 2024-T4
Rotor blade	Composite + Titanium Nose Cap
Fuel Tank	Kevlar

7.4 Weight and Balance

The weight of each GTT component was derived using the weight equations provided in the HESCOMP manual [18], with exception to the flight crew, payload, and fuel. The weights of the flight crew and payload were specified in the RFP. The fuel weight was calculated during tandem sizing. The longitudinal station data for each of the components is determined by the center of gravity. The zero station is taken at the nose of the vehicle and the

zero waterline is taken at the bottom of the fuselage. The datum line between the rotors is 463 inches from the zero station. The component weight breakdown and station data for the GTT are presented in Table 16 and the longitudinal C.G. calculation is shown in Table 17. Figure 38 shows the relationship of the center of gravity as the vehicle is loaded. The maximum travel of the C.G. for the GTT’s FCS mission is 25 inches.

TABLE 16: COMPONENT WEIGHT

Components	Weight, lbs	Arm, in	Components	Weight, lbs	Arm, in	Components	Weight, lbs	Arm, in
Wing	0	0	Nacelle	3309	620	Pilot	600	36
Rotor	9621	463	Air Induction	1028	620	Crew	440	108
Aux. Prop.	227	0	Drive System	9708	720	Fuel	11183	400
Body Group	9697	433	Rotor Control	4801	463	Fuel Reserve	1833	430
Alighting Gear	2351	389	Flight Control	3561	96	Empty Weight	51189	473
Engine	3848	620	Avionics	1200	60	Misc	1647	463
Engine Mount	447	620	Payload	40000	440	Gross Weight	105245	

TABLE 17: LONGITUDINAL C.G. CALCULATION.

	Individual Weight (lbs)	Compiling Weight (lbs)	Station (in)	Moment (in-lb)	Compiling Moment (in-lb)	Station (in)	Waterline (in)
Total Empty Weight	51189	51189	494	25295969	25295969	494	112
Pilots	600	51789	36	21600	25317569	489	111
Crew	440	52229	108	47520	25365089	486	111
Fuel Weight	11183	63412	400	4473280	29838369	471	121
20min Fuel Reserve	1833	65245	430	788121	30626491	469	122
FCS	40000	105245	440	17600000	48226491	458	94
Final Location		105245				458	94

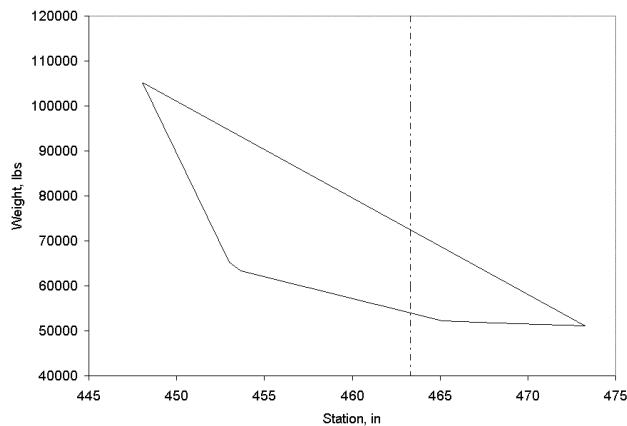


FIGURE 38: LONGITUDINAL CENTER OF GRAVITY ENVELOPE

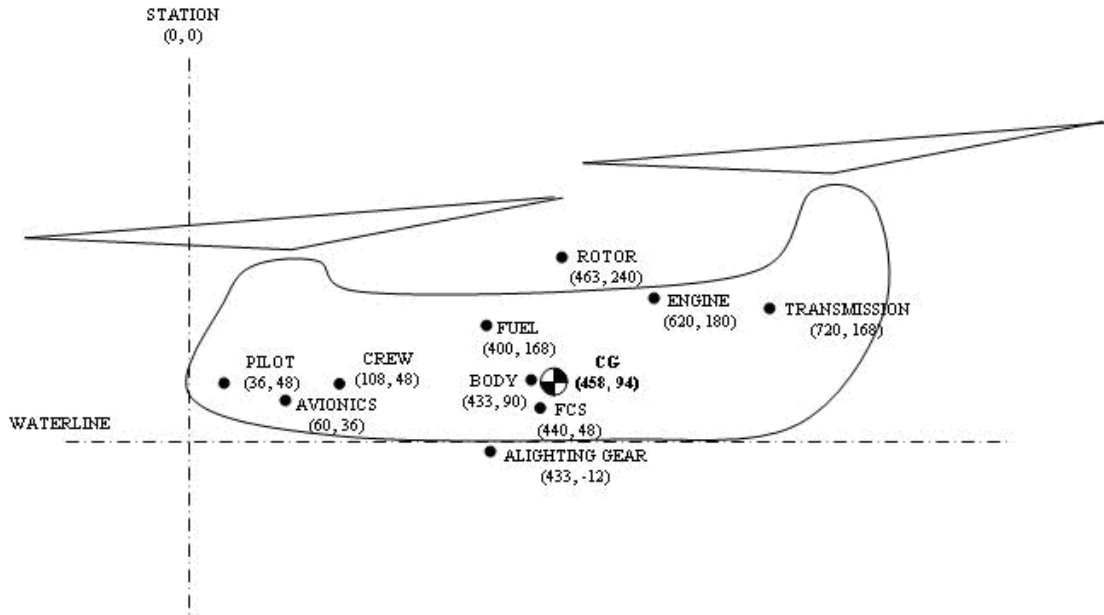


FIGURE 39: COMPONENT CENTER OF GRAVITY

7.5 Design Flight Speeds

The design flight speeds for the GTT are presented in Table 18. The ratio of the design maximum level flight speed, V_{max} , to the design limit flight speed, V_{DL} does not exceed 1.15 for a heavy lift helicopter as specified in Reference [7].

TABLE 18: DESIGN FLIGHT SPEEDS

	GTT Design Flight Speed, kts		GTT Design Flight Speed, kts
V_{DL}	193	V_{end}	115
V_{cruise}	168	V_{rocmx}	115

7.6 Load Factors

The load factors for the selected loading conditions are presented in Table 19. The load factor for the GTT landing condition was applied to the fuselage structure at only one landing gear location, because it is difficult to contact two or more of the landing gear at the same time while touching down during landing.

TABLE 19: LOAD FACTOR

Maneuver	Load Factor	Maneuver	Load Factor
Pullup at DGW	2.5	Landing (10 fps)	2.5
Pushover	-0.5	Static Ground	1

7.7 V-N Diagram

The V-N diagram presents the estimated flight loads at the different flight maneuvers.

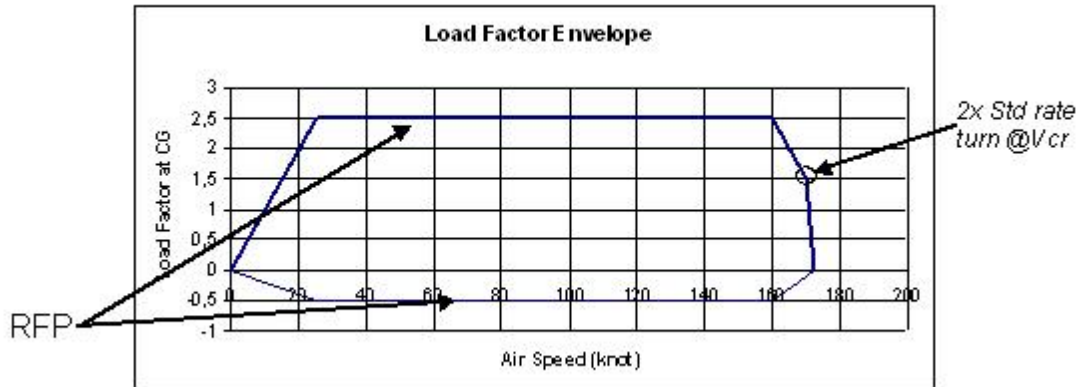


FIGURE 40: V-N DIAGRAM

7.8 Blade Structural Design

7.8.1 Blade

The primary structure of the rotor blade is composite. An all composite blade was selected for several reasons. First, fabricating composite blades allows smooth blending from one airfoil section to the next including the swept tip section. Second, the weight of the blades will be reduced compared with a metal blade. Finally, composite blades have a much greater fatigue life than metal blades. The composite web has longitudinal, lateral, and 45° fibre orientations. This will provide the required strength and stiffness in flapping and torsion. There are also small ducts that run the length of the blade that direct warm air for the purpose of de-icing. A titanium nose cap will cover the external surface of the blade. The nose cap provides mainly erosion protection and some additional torsion and bending stiffness.

7.8.2 Root End Retentions and Tip Closure

The root end retention is integrated into the composite blade structure and includes steel inserts for all connection points. As far as tip closure is concerned, fixed weights will be mounted to set the inertia of the blades to the aimed value and reduce vibrations by balancing the four blades.

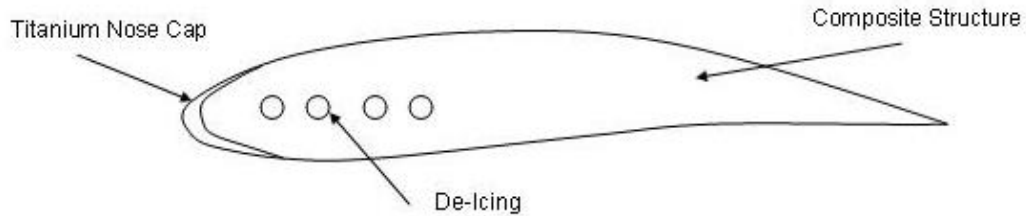


FIGURE 41: BLADE STRUCTURE

7.9 Alighting Gear

The location of the alighting gear affects the landing attitudes for symmetric and asymmetric landings, roll over, tip back, and tip forward angles. Another concern is the large payload this vehicle is required to hoist into the cargo section. Due to the load handling previously described, the alighting gear must remain clear of the FCS during pickup. Therefore, the forward gear is placed at station 216 and the aft gear is placed at station 564. Both of these stations are outside of the pilot and crew compartment to ensure the gear will not penetrate into these areas during a crash. The following figures show the front and aft alighting gear.



FIGURE 42: FRONT AND AFT ALIGHTING GEAR

Once the center of gravity is defined, the roll over angle can be calculated. The tip back and forward angles can also be calculated using the CG data and the location of the alighting gear. Table 20 shows the roll over angles for the GTT.

TABLE 20: ROLL OVER ANGLES

Roll Over	Tip Back	Tip Forward
39°	46°	64°

7.10 Load Handling

To expedite the pickup and drop off of the FCS vehicle, the cargo section of the GTT is equipped with bomb bay type cargo doors. For the FCS delivery mission there is no floor section in the cargo bay. This facilitates the GTT hovering above or landing over the FCS during pickup. Hoists are then attached to the FCS and it is pulled up into the cargo bay. Special slots will be needed on the sides of the FCS to mate with the internal locking mechanism. The purpose locking the FCS into the cargo bay is to stabilize it during flight and relieve tension from the hoist cables. A conceptual diagram of the FCS locking mechanism and loading configuration are shown in the following figure.

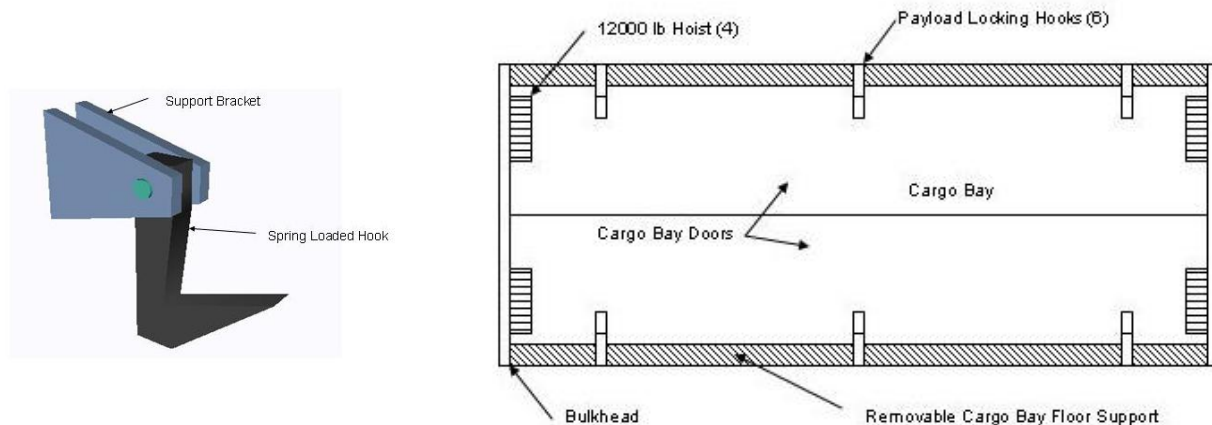


FIGURE 43: FCS LOADING CONFIGURATION

7.11 Fatigue

Due to the environment rotorcraft operate in, fatigue must be considered for all components during the design. According to Minor's Rule, during normal flight conditions the loads applied to each component must remain below

a statistically reduced stress versus cycle curve for that component material. The Figure 44 shows a representation of the stress versus cycles for a component that has an acceptable fatigue life.

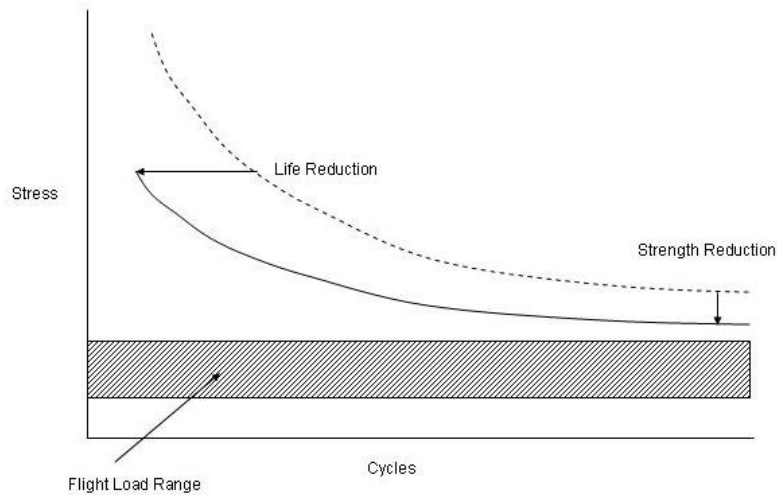


FIGURE 44: FRONT AND AFT ALIGHTING GEAR

8 Stability and Control

Design of the GTT necessitates adequate stability and control (S&C) for performing its missions. These characteristics should be analyzed across the entire flight envelope, with special consideration that helps to determine design parameters given to hover and cruise. Presented here is a summary of the process we planned to use for the GTT S&C and some of the early results and specification of the flight control system (FCS).

8.1 Requirements

The S&C of the GTT ensures safe and proper functioning of the aircraft while in its modes of operation. There are certain to be conditions where the aircraft dynamics are unstable—or possess a tendency to diverge from their current states when disturbed—and under these regions stability augmentation should be applied to either limit or eliminate the risk of instability. First, however, these regions are identified utilizing guidelines put forth from authorized sources that outline specific handling qualities desirable of rotorcraft. Interpreting the body dynamics of the GTT in terms of these handling qualities is the final step in analyzing the S&C of our design. Once this is completed the process of determining and assigning dynamic characteristics, like hinge offset, and controller

properties, like PD gains, can be iterated through again and again. Actual handling qualities requirements are organized in a number of extensive and thorough documents. ADS-33C is the most recent and complete source besides those explicitly stated in the RFP. An interpretation of these requirements is organized and presented in Table 21 and served as the motivator of our planned S&C design for the GTT.

TABLE 21: STABILITY AND CONTROL REQUIREMENTS

Stability	Controllability
Level 1 Handling Qualities	Control During Autorotation to Survivable Landing
Conforms to Standards (ADS-33)	Sufficient Control Power
Benign Ground & Air Resonance	Sustained Turn Rate Capability of 2x SRT
Maintainability	Precision Hover (Cargo Handling)
Facilitate Basic Maintenance of Flight Controls	Control Augmentation for Adverse Weather & Night

Several tools should be used to jointly create and model the nonlinear dynamic system of the GTT. A general specification of the GTT provides one with reasonable data for necessary variables, such as blade mass properties, in modeling this dynamic system [19]. The GTT characteristics can then be supplied to commercial off-the-shelf software, called Flightlab™, where a model of the rigid body dynamics of the tandem helicopter can be created. Flightlab™ was used in the S&C analysis of the GTT for determining the open and closed loop characteristics, linearizing the system about particular points, and for creating a first cut at simplified stability augmentation system (SAS) and control mixing. It was also our intent to utilize Matlab™, a versatile and flexible software tool, for validating and modeling the GTT in a parallel manner. A brief summary of the various assumptions and techniques applied to components of the mathematical models for the GTT are listed in Table 22.

TABLE 22: MODEL ASSUMPTIONS

Forward & Aft Rotor	Airframe
Blade Element Techniques for Rotor Dynamics	Rigid Fuselage
Articulated Rotor Hub	Non-Uniform Airloads
Quasi-Steady Airfoils	Flight Control
Peter/He 3-State Inflow Model	Simplified Control Feedback providing SAS
Propulsion	
Ideal engine	

8.2 Stability Analysis

8.2.1 *Methods Description*

The S&C analysis of the GTT was focused about two areas: body dynamics and rotor dynamics. Inflow dynamics were generally ignored except when generating mathematical models of the rigid body system. Within the body dynamics of the GTT, there are six degrees of freedom (DOF) that correspond to translational and rotational motion or acceleration. We chose to describe this 6-DOF system using twelve states, however, only eight of those states are used for the stability analysis. The body dynamics system is supplied with only four inputs from the user—cyclic, collective, and pedal (directional) commands—and these four controls must be appropriately mixed into the three controls of each rotor (6 total). The rotor dynamics of the rigid body were modeled using 1-DOF blade flapping and two states.

Modeling of the GTT continues with defining formula for the rotor blade dynamics, principally flapping, where a quasi-steady assumption should be used to simplify analysis of the rigid body. Analytical expressions for the forces and moments acting on the entire body can be found, and, using those expressions, systems of equations can be organized to determine an equilibrium/operating point where the aircraft is “trimmed”. Our plan was to complete this modeling of the GTT using numerical methods in Flightlab™ and analytical expression in “in-house” codes using MATLAB. Part of our validation was to compare both types of results with CH-47 data.

After success in modeling the GTT, trim conditions can provide an operating point about which to linearize and then examining stability. Linearization relies on the use of small perturbation theory, where system responses are limited to small deviations of trimmed conditions—this limitation exists because the GTT and all rotorcraft are inherently nonlinear. The GTT linear system used for stability analysis consisted of eight states, four controls, and six outputs. From this reduced order representation of the nonlinear system, necessary stability derivatives can be extracted and used for determining GTT handling qualities. As the system is linearized about trim conditions across its flight envelope, trends can be developed. Finally, eigenvalues of the stability matrix depicting the modes of the GTT at a particular flight condition can be determined and also used for comparison against handling qualities requirements.

8.2.2 Trim Analysis

Results of preliminary trim analysis are presented in Figure 45 for flight conditions from hover to cruise speed. These results shown assume symmetric flight with zero sideslip and no gust. These results are evidence that the GTT is controllable across its operational envelope, but the poor performance requires improved stability augmentation, control mixing, and perhaps redesign of some elements of the hub design.

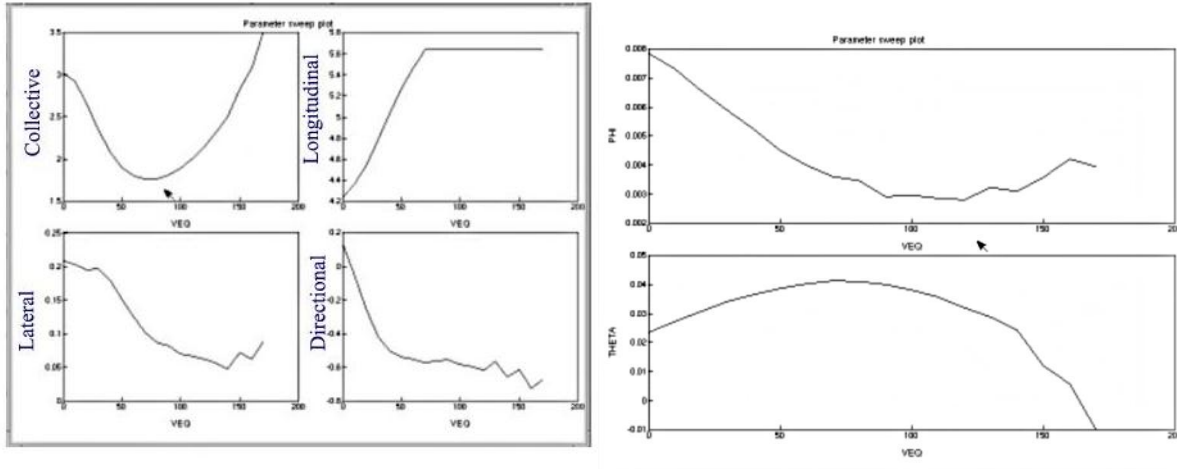


FIGURE 45: TRIM ANALYSIS RESULTS

8.2.3 Linearized System Results

Presented in the following equations are preliminary results for linearization of the GTT rigid body dynamics in hover. These equations are evidence that our linearization attempts were successful, and can be used for further S&C analysis.

$$\begin{aligned}\partial\dot{x} &= A\partial x + B\partial\delta \\ \partial\dot{x} &= \dot{x} - \dot{x}_{trim} = \dot{x} - 0 = \dot{x} \\ \partial x &= x - x_{trim} \\ \partial\delta &= \delta - \delta_{trim}\end{aligned}$$

$$x_{trim} = \begin{bmatrix} p^* \\ \phi^* \\ q^* \\ r^* \\ \theta^* \\ u^* \\ v^* \\ w^* \end{bmatrix} = \begin{bmatrix} -0.022952 \\ 0.011773 \\ 0.008922 \\ -0.014753 \\ 0.023491 \\ 0.402214 \\ -0.042652 \\ -0.00205 \end{bmatrix} \quad \delta_{trim} = \begin{bmatrix} \delta_a^* \\ \delta_c^* \\ \delta_e^* \\ \delta_p^* \end{bmatrix} = \begin{bmatrix} 0.212695 \\ 3.019582 \\ 4.235785 \\ 0.118204 \end{bmatrix}$$

$$A = \begin{bmatrix} -0.0005 & -0.0150 & -0.0000 & -0.0000 & -0.0000 & 0.9999 & 0.0003 & 0.0235 \\ 0.0150 & -0.0000 & -0.0000 & -0.0000 & -0.0000 & -0.0000 & 0.9999 & -0.0118 \\ -0.6982 & -32.1889 & -0.0052 & -0.0011 & 0.0310 & -0.0729 & 1.4127 & 0.5859 \\ 31.7756 & -0.0025 & 0.0104 & -0.0152 & 0.0083 & -1.7368 & -0.0662 & -0.4666 \\ -0.3565 & -0.7551 & -0.0106 & -0.0101 & -0.3798 & 0.3200 & 0.3108 & 0.1669 \\ -0.1786 & 0.0028 & -0.0001 & -0.0079 & -0.0003 & -2.5491 & -0.4627 & 0.0034 \\ 0.0424 & -0.0043 & -0.0019 & -0.0010 & -0.0003 & 0.0126 & -0.9158 & 0.2384 \\ 0.0363 & -0.0005 & -0.0007 & 0.0007 & -0.0003 & 0.2099 & 0.2599 & -0.0704 \end{bmatrix}$$

$$B = \begin{bmatrix} 0 & 0 & 0 & 0 \\ 0 & 0 & 0 & 0 \\ 0.0293 & 0.272 & 0.2913 & -0.0373 \\ -1.0882 & -0.0152 & -0.0962 & 0.049 \\ -0.0183 & 0.0461 & -12.3848 & -0.0094 \\ -0.677 & 0.0576 & 0.046 & 0.3146 \\ -0.0029 & 0.3453 & -0.0065 & -0.0071 \\ 0.0517 & -0.0552 & -0.0043 & -0.1915 \end{bmatrix}$$

8.2.4 Eigenvalue Analysis

Early attempts at determining the eigenvalues of our linearized GTT proved successful. Figure 46 illustrates the root locus plot of the various modes of the GTT in hover. As seen in the figure, further stability augmentation should be included to stabilize the one unstable mode and one poorly damped mode.

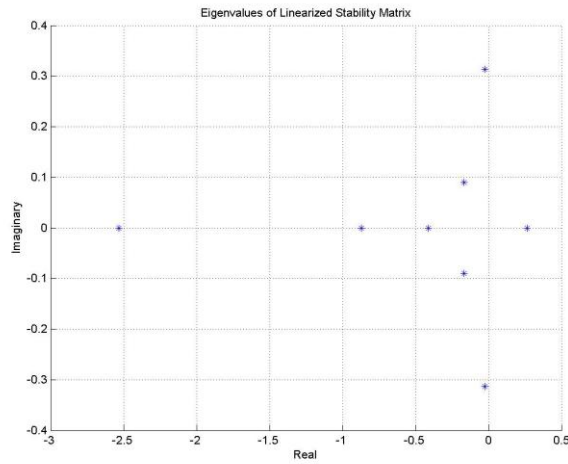


FIGURE 46: ROOT LOCUS

8.2.5 Static Stability Analysis

Because the GTT could be linearized about various flight conditions, specific stability derivatives available in the stability matrix offered some insight into the static stability of the GTT. Table 23 presents estimates of these stabilities from the linearization shown in Figure 46.

TABLE 23: STATIC STABILITY ANALYSIS

Speed Stability	AOA Stability	Dihedral Effect	Directional Stability
Negative	Negative	Positive	Positive

8.3 Flight Control System

The GTT flight control system will utilize the state-of-the-art adaptive neural network controller. This flight controller exhibits many general advantages, including lower control design and testing times, lower cost through simulation, and smooth, easy transition from one flight regime to another—a problem with gain scheduling.

The shipboard mission requirements of the aircraft require precise flying in both VFR and IFR conditions. To lessen the workload of the pilot and provide for this precision, an Attitude Command Attitude Hold (ACAH) type of control will be available during IFR conditions for longitudinal control. A Rate Command Rate Hold (RCRH) will be available for longitudinal control in VFR and the lateral and directional control for both VFR and IFR conditions. Figure 47 generalizes the architecture of the adaptive neural network FCS.

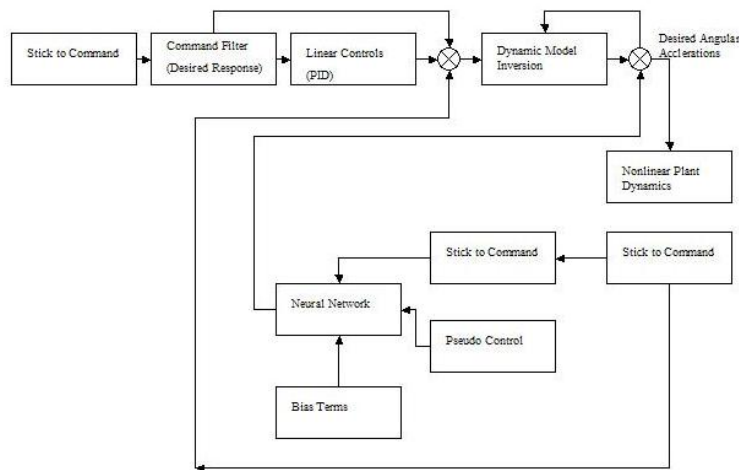


FIGURE 47: CONTROLLER ARCHITECTURE

8.4 Maintainability

The flight control system will be designed using fly-by-wire techniques. There are several significant benefits by choosing this form of implementation. First, the weight of mechanical components is decreased. Second, the flight control system provides better integrity and availability through redundancy in a triplex or quadplex system. Third, the availability for upgrades is rapidly increased.

9 Engine Selection

The engine selection for the GTT began with determining the total installed power required at sea level in the tandem sizing tool. The specific condition that sized the GTT engine was the OEI condition in hover provided in the RFP mission profile. The total installed power required from our sizing of the GTT was 23,132 HP at sea level. We researched available engines that could meet our performance requirements—assuming that four engines would be needed. Table 24 presents the data for these various engines.

TABLE 24: ENGINE DATA

Model	Designation Type	Number of Fan/Compressor Stages	Number of Turbine Stages LP/HP	MCP at SL	S.F.C. at MCP Setting
AE 3007C/CI	AFF	1,14	2,3	6,764 lb.t	0.63
T56-A427	AFP	14	4	5,823 shp	0.47
AE 1107 C	AFS	14	2,2	6,150 shp	0.41
T56-A16	AFP	14	4	4,591 shp	0.54
AE-2100D2	AFP	14	2,2	4,591 shp	0.46

Based on the available data, we selected the AE 1107C. With four AE 1107C engines the total installed horsepower will be 24,600 HP—slightly more than what is required. Additionally, this engine gives a very good specific fuel consumption (SFC) of 0.41 at the maximum continuous power rating—our selected engine condition for the OEI sizing requirement. Figure 48 shows a picture of a AE 1107C engine. All the information for the selected engine was found in references [20] and [21].

9.1 Engine Details

The AE-1107 provides the GTT with a modern, rugged power plant. Advanced technology features for the engine include all-axial high efficiency turbo-machinery components, only four main rotor bearings, positive sump scavenging, modular construction and independent Full Authority Digital Engine Control (FADEC). The AE 1107C is capable of developing over seven shaft horsepower per pound of weight—the highest ratio of any engine in its class. Its modern design offers a versatile core common to the AE 2100 turboprop and AE 3007 engines. Some useful characteristics of the engine are given in Table 25.

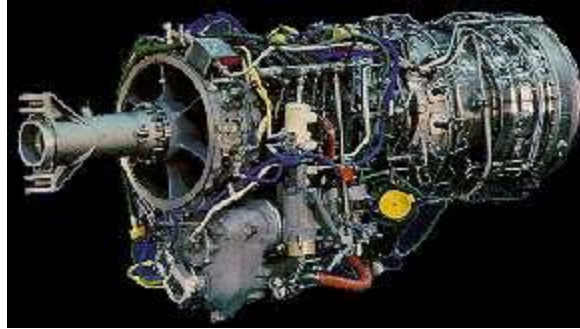


FIGURE 48: AE-1107C ENGINE [20]

The two-shaft axial design consists of a 14-stage compressor followed by an effusion-cooled annular combustor, a two stage gas generator turbine and two-stage power turbine. The engine features six rows of variable compressor vanes, a self contained oil system, modular construction, and on-condition maintenance capability.

TABLE 25: AE-1107C SPECIFICATION [20,21]

AE 1107 C Specifications	
Max. Envelope Diameter, in	34.2
Length, in	77.9
Width, in	28.8
MCP, shp	6,150
S.F.C.	0.41
Max. Turbine Temperature, F	2,200
Engine Dry Weight, lbs	971

9.2 Engine Installation and Power Losses

The engines and transmission of the GTT were placed 50 ft from the nose towards the aft of the rotorcraft. This location was chosen because of structural and stability constraints. Estimated power losses are shown in Table 26. More accurate numbers can be determined through flight testing and a detailed description of the engine's installation.

TABLE 26: POWER LOSS ESTIMATION [7]

Estimated Power Losses	
IPS/icing	4%
Transmission	5%
Gear reduction	2%

10 Transmission

The transmission for the GTT was based on the CH-47D drive train. The GTT drive train consists of four engines connected to the combining transmission box, and the output of the combining transmission is connected to the fore and aft bevel gears. These gears convert the horizontal shaft rotations to vertical rotations of the shaft. The two-stage planetary gear system is connected to the fore and aft vertical shafts, and the rotors are connected to the spindle of the second stage planetary gear. The four-engine combining transmission box consists of two combining transmission boxes arranged in series as shown in Figure 49.

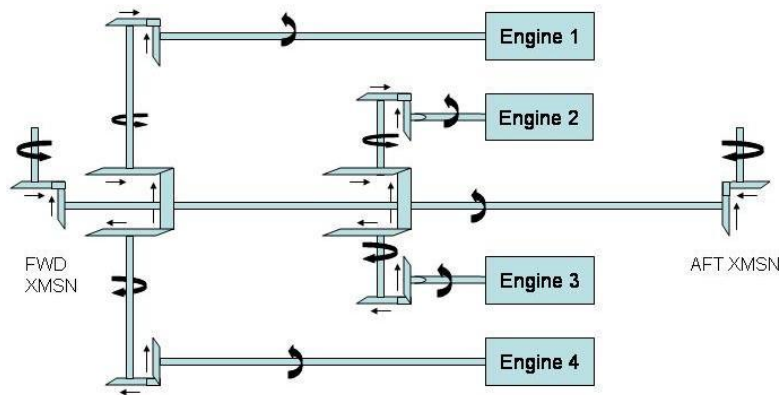


FIGURE 49: FOUR ENGINE COMBINER BOX

The planetary gear system was selected because the planetary gears have an advantage in terms of weight reduction. The load transmitted by the sun is shared by the planets (pinions), so the pinions can be smaller in size. The GTT transmission was sized based on the maximum horsepower required for a given mission segment flight condition. The limiting torque of the engine and rotor was computed using the relationship that the power supplied by the engine equals the power absorbed by the rotors. The results are shown in Table 27. A comparison of single speed and dual speed transmissions was investigated. In addition, the results of stress analysis and shaft analysis are presented.

TABLE 27: POWER AND TORQUE RESULTS

Maximum HP	Engine Torque, ft lb	Torque per Rotor, ft lb
13,900	52,869.5 (Limiting Value)	2,964,195.4

10.1 Single Speed Transmission

The diameters, speeds, heights, and face width of the gears are sized using the following procedure. The planetary gear system consists of the sun gear (input), the ring gear (fixed), and the arm carrier (output). The arrangement is shown in Figure 50.

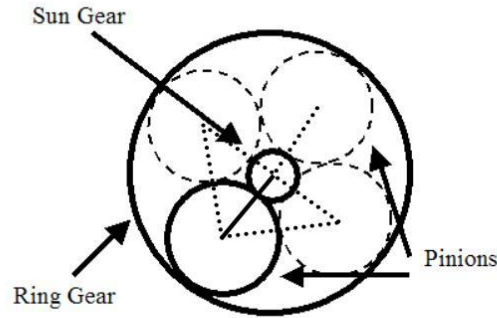


FIGURE 50: PLANETARY GEAR ARRANGEMENT

Assuming, the sun is rotating counter clockwise, the ratio of the ring gear speed to the sun gear speed is expressed relative to the arm carrier, because the arm carrier is moving. The planetary train factor was defined as

$e_{sun-ring} = \frac{n_{ri} - n_{ai}}{n_{si} - n_{ai}}$, where n_{si}, n_{ai}, n_{ri} are the speeds of the sun, arm, and ring gears respectively. The ring gear is

fixed, $n_{ri} = 0$. Therefore, $\frac{n_{ai}}{n_{si}} = \frac{N_{si}}{N_{ri} + 1}$, where N_{si}, N_{ri} are the teeth of the sun and ring, respectively.

Furthermore, $e_{sun-pinion} = \frac{n_{pi} - n_{ai}}{n_{si} - n_{ai}}$, where n_{pi} is the speed of the pinion and N_{pi} is the teeth of the pinion.

Therefore, $e_{sun-ring} = \frac{-N_{si}}{N_{ri}}$ and $e_{sun-pinion} = \frac{-N_{si}}{N_{pi}}$, and the negative sign implies that rotation of the pinion and the

ring are opposite to the sun. Based on these expressions, $n_{pi} = \frac{N_{si}}{N_{pi}} (n_{ai} - n_{si}) + n_{ai}$.

There are several constraints that need to be considered for proper meshing of the teeth in the GTT. These are constraints demand that $N_{ri} = N_{si} + 2N_{pi}$, $N_{si} + N_{ri} / (\text{no. of pinions})$ must equal an integer value and also that, for a given planetary gear system, diametrical pitch is the same for the ring, pinion, and sun. Results for the single RPM = 146.746 of the GTT transmission are shown in Table 28 and Table 29. Two pinions were used for the first

stage, and four pinions were used for the second stage. A diametrical pitch of 2.7 and 5.1 were assumed for the first and second stage respectively.

TABLE 28: GEAR PARAMETERS

	Sun	Ring	Pinion
	Diameter, inch		
1 st Stage	9.26	25.56	8.15
2 nd Stage	5.88	28.63	11.37
	Teeth		
1 st Stage	25	69	22
2 nd Stage	30	146	58
	Speed, RPM		
1 st Stage	2000	0	-746.75
2 nd Stage	714.29	0	-146.81
	Face Width, inch		
1 st Stage	2.97	11.51	2.97
2 nd Stage	15.68	17.17	15.68
	Height, inch		
1 st Stage	0.83	0.83	0.83
2 nd Stage	0.44	0.44	0.44

TABLE 29: GEAR RATIO AND TORQUE

Bevel Gear Ratio	1 st Stage Planetary Gear Ratio	2 nd Stage Planetary Gear Ratio	Overall Ratio
3:1	2.8:1	4.8675:1	40.887:1
	Sun	Ring	Pinion
Torque 1 st Stage, ft lb	203,147	-544,080	-544,080
Torque 2 nd Stage, ft lb	284,405	-1,384,000	-1,384,000

10.2 Two Speed Transmission

A two speed planetary gear transmission for the GTT was investigated instead of a variable speed because the variable speed utilizes traction or friction to drive pulleys, which are variable diameter pulleys and transmit less power. They are less efficient because the normal component of force is used to produce the tangential component. Additionally, there is a weight penalty associated with the variable speed drive—unless a split torque transmission is used and the power is shared between the sun and the ring. Because of all these factors, a dual speed transmission where the sun is the input, the arm is the output, and the ring speed is varied was analyzed for the GTT. The formulas used were obtained from reference [22]. The procedure for this transmission begins with engaging the

clutch. Power is supplied to the 2nd stage ring gear while a break is put on 1st stage ring gear; this results in a constant rotor RPM. Next, the reduction ratio is increased by 30% to reduce the rotor speed by as much as 30%. The speed change is achieved by engaging the clutch, so that power is supplied to the 1st stage ring gear and now a break is put on 2nd stage ring gear. The results of this dual speed process are shown in Table 30. The symbols S, R, and P denote the teeth of the sun, ring, and pinion gears. The symbol RR represents the reduction ratio.

TABLE 30: TWO SPEED TRANSMISSION RESULTS

Input	R1 Fixed/R2 Free	R2 Fixed/R1 Free	Speed Change
S1 = 14	RR1 = 13.629	RR2 = 17.718	
P1 = 81	RPMOUT = 146.746	RPMOUT = 112.881	23%
R1 = 176	RPMR1 = 0	RPMR1 = -39.51	
R2 = 44	RPMR2 = 38.05	RPMR2 = 0	
P2 = 15	RPMP1 = -318.86	RPMP2 = 331.12	
Number of Pinions = 2 RPM SUN = 2000			

Even though analysis of the dual speed transmission proved favorable for the GTT, it did not offer enough benefit against the weight penalty associated with the large dimensions of the first stage ring gear and first stage pinion, as shown in Table 31.

TABLE 31: GEAR DIAMETER

Diameter, inch				
Sun	Ring 1 st Stage	Ring 2 nd Stage	Pinion 1 st Stage	Pinion 2 nd Stage
5.19	65.19	8.63	30	2.94

10.3 Stress Analysis

Calculation of the GTT geometry factors, transmitted forces, torques, bending stress, and contact stress was performed using AGMA formulae obtained from reference [23].

10.3.1 Geometry Factors

The Geometry factors were computed using AGMA formulae. The results of their application are shown in Table 32. M_{c_i} , Z_i , M_{n_i} , I_i , J_i , and M_{G_i} represent the contact ratio, length of line of action, load sharing factor, geometry factors for the sun-pinion, and speed ratios respectively. The symbol i ($=1,2$) in each of these variables represents the index of the stages.

TABLE 32: GEOMETRY FACTORS

Mc1	Mc2		Z2	MN1	MN2	I1	I2	J1	J2	MG1	MG2
1.05	0.5286	1.15	0.306	1	1	0.085	0.0547	0.34	0.425	1.136	0.517

10.3.2 Force Analysis

The tangential force of the GTT drive system design was computed by dividing the HP per rotor by the pitch line velocity. The resultant force acts along the pressure line at an angle $\phi=20^\circ$ to the horizontal tangent line. When resolved, this is the resultant force that a specified gear exerts on its mating gear. The forces are further resolved to obtain the radial and total force. The results are shown in Table 33.

TABLE 33: FORCE ANALYSIS RESULTS

	Radial Force, lbs	Tangential Force, lbs	Total Force, lbs	Transmitted Torque, ft lb
1 st Stage				
Sun - Pinion	24,313	66,800	71,087	25,771
Pinion - Ring	7,752	21,299	22,666	15,390
2 nd Stage				
Sun - Pinion	44,303	121,720	129,533	29,834
Pinion - Ring	17,600	48,356	51,459	22,914

10.3.3 Stress Analysis

The bending and contact stresses of the GTT drive system were calculated using AGMA stress formulae. The pinion material used was carbonized and case hardened steel. The material used for the ring and sun gear was A5 steel. Results for these stresses are shown in Table 34.

TABLE 34: CONTACT AND BENDING STRESSES

Sun - Pinion			
Maximum Contact Stress, psi	Maximum Bending Stress, psi	Allowable Contact Stress, psi	Allowable Bending Stress, psi
1 st Stage: 554,685	1 st Stage: 324,030	170,000	48,000
2 nd Stage: 332,824	2 nd Stage: 158,330		

Factors of safety for the bending stress were 6.75 and 3.3 for the first and second stages respectively. The factors of safety for the contact stresses were 3.26 and 1.96 for the first and second stage respectively.

10.4 Shaft Analysis

The GTT shaft natural frequency varied inversely with the length of the shaft. Longer lengths meant smaller natural frequencies and a greater the risk of running into resonance. Therefore, a critical length was determined for the operating output speed of the combiner (6000 RPM), and it was compared with the length of the forward shaft. The criterion for this design parameter was that the actual length be less than the critical length. The length of the original shaft was 48.22 ft and the critical length was 26.73 ft. Therefore, it became necessary to cut the shaft into three divisions. The first bending speed was computed as 16620.3 RPM. This shaft analysis was only done for the forward shaft. A high fidelity analysis would involve stress analysis to determine an appropriate thickness of the shaft, and the process would involve computing the natural frequencies of the aft shaft and vertical shafts.

11 Cost Analysis

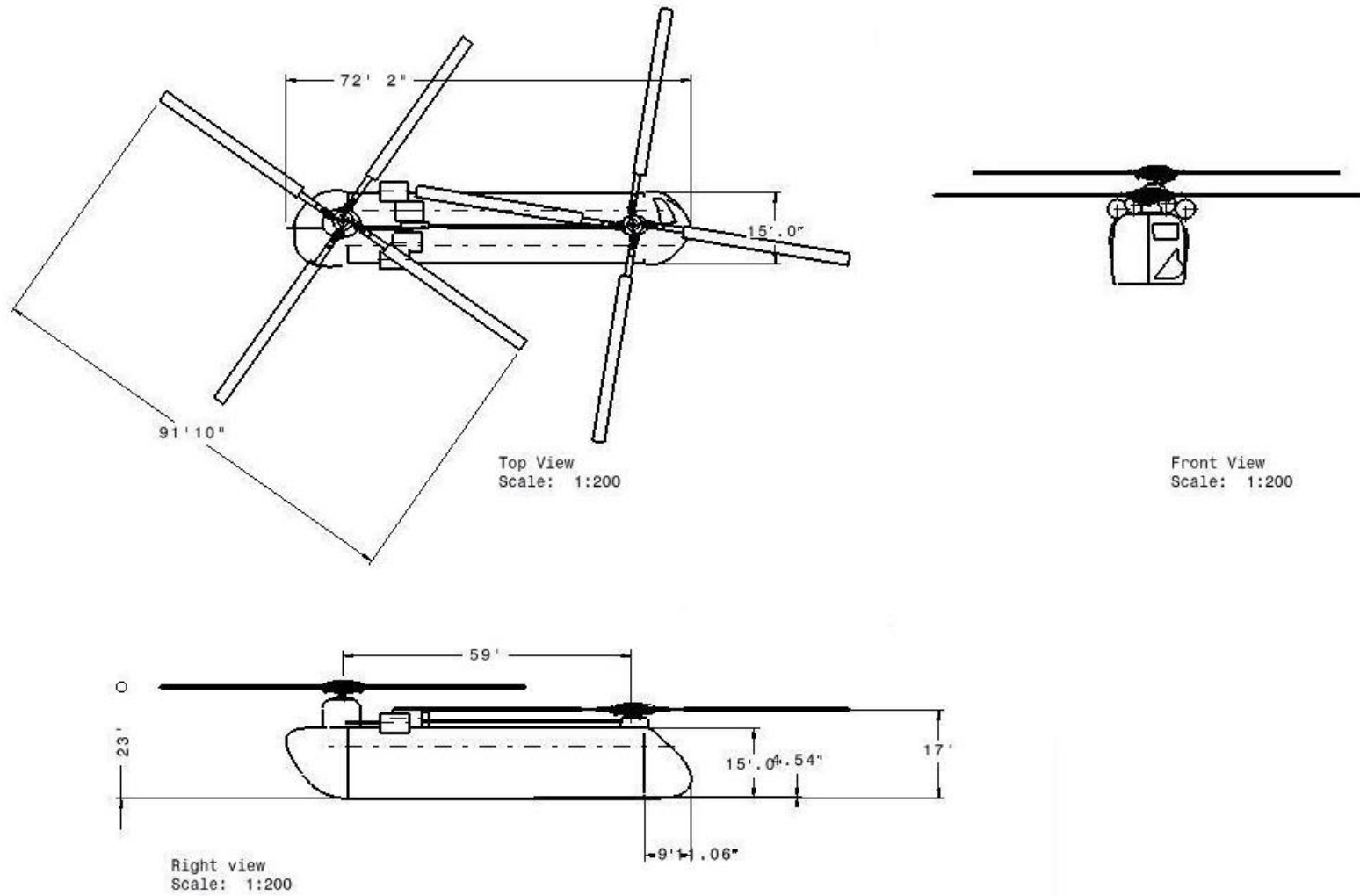
As stated in the RFP and our OEC, the primary measure of merit for the GTT is the time it takes to deliver four FCS vehicles over acquisition cost. Because the value of our vehicle's design depends on managing the negative factors that inflate acquisition cost, an important goal in design of the GTT was to minimizing the overall cost of our vehicle. To do this however, we needed another way to analyze the cost of our design.

With this goal, the team analyzed the cost of the GTT using the Bell Helicopter Cost Model, a rotary wing cost analysis tool developed by the Bell Helicopter Corporation. The tool uses a multi-level parametric approach to estimate development and recurring production costs. The program requires user inputs in aircraft configuration, intended use, percent of new components, and labor rates. Additionally, the Bell Cost Model allowed our team to customize a model by entering exact weights for the various components that comprise the GTT.

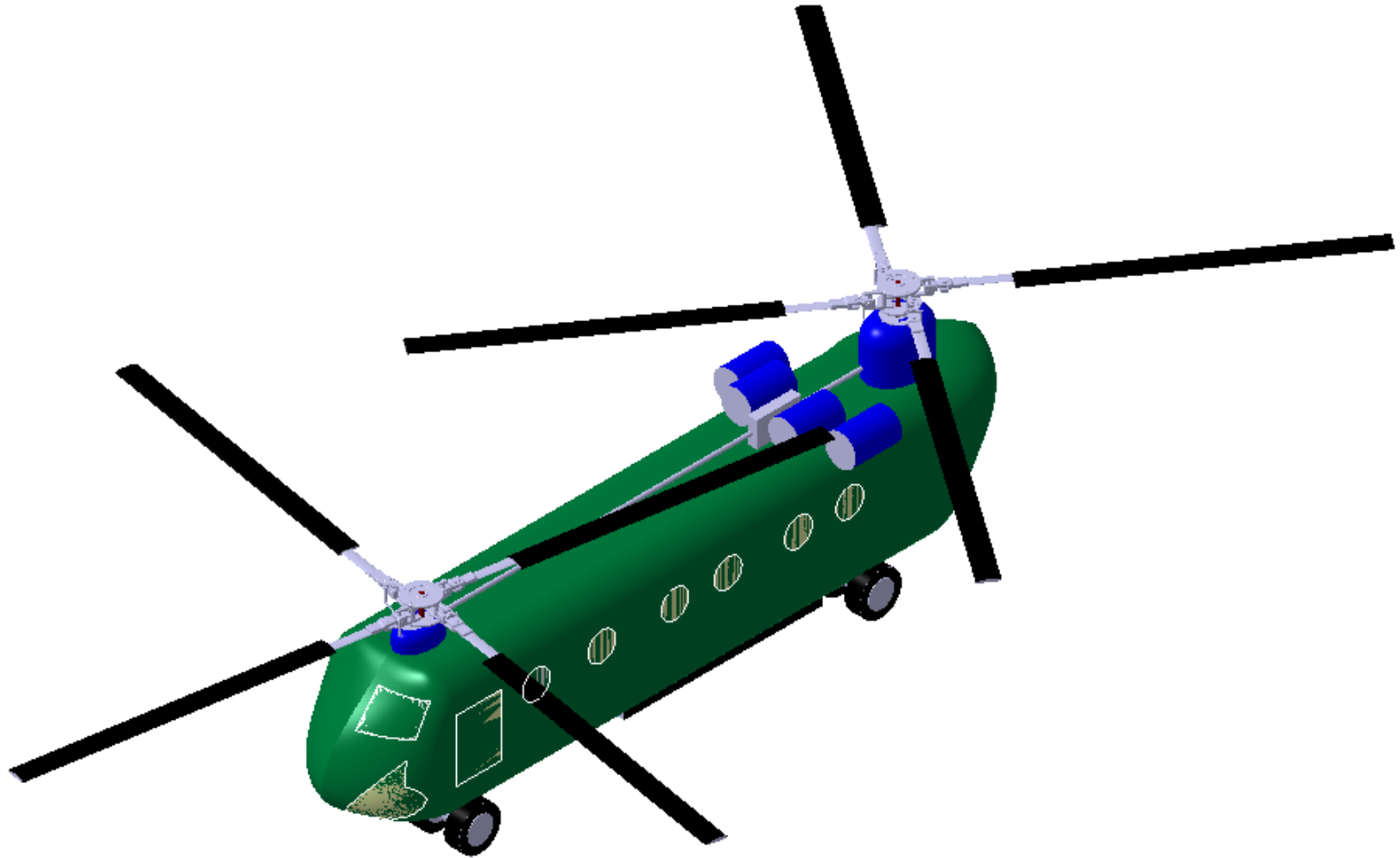
The overall production for the GTT was specified in the RFP to be "200 aircraft delivered over a 15 year manufacturing period." Based on this projection and using the Bell Cost Model, we calculated the acquisition cost per airframe for the GTT to be \$47,465,000. The cost of the GTT is low when compared to similar heavy lift VTOL aircraft—none of which have the capability of transporting a 20-ton FCS vehicle. The direct operating cost of the GTT is relatively high, however, at \$6,156 per flight hour. This value was an estimate based on historical data, and it is a function of fuel consumption as a fixed percentage of direct operating cost.

12 CATIA Drawings

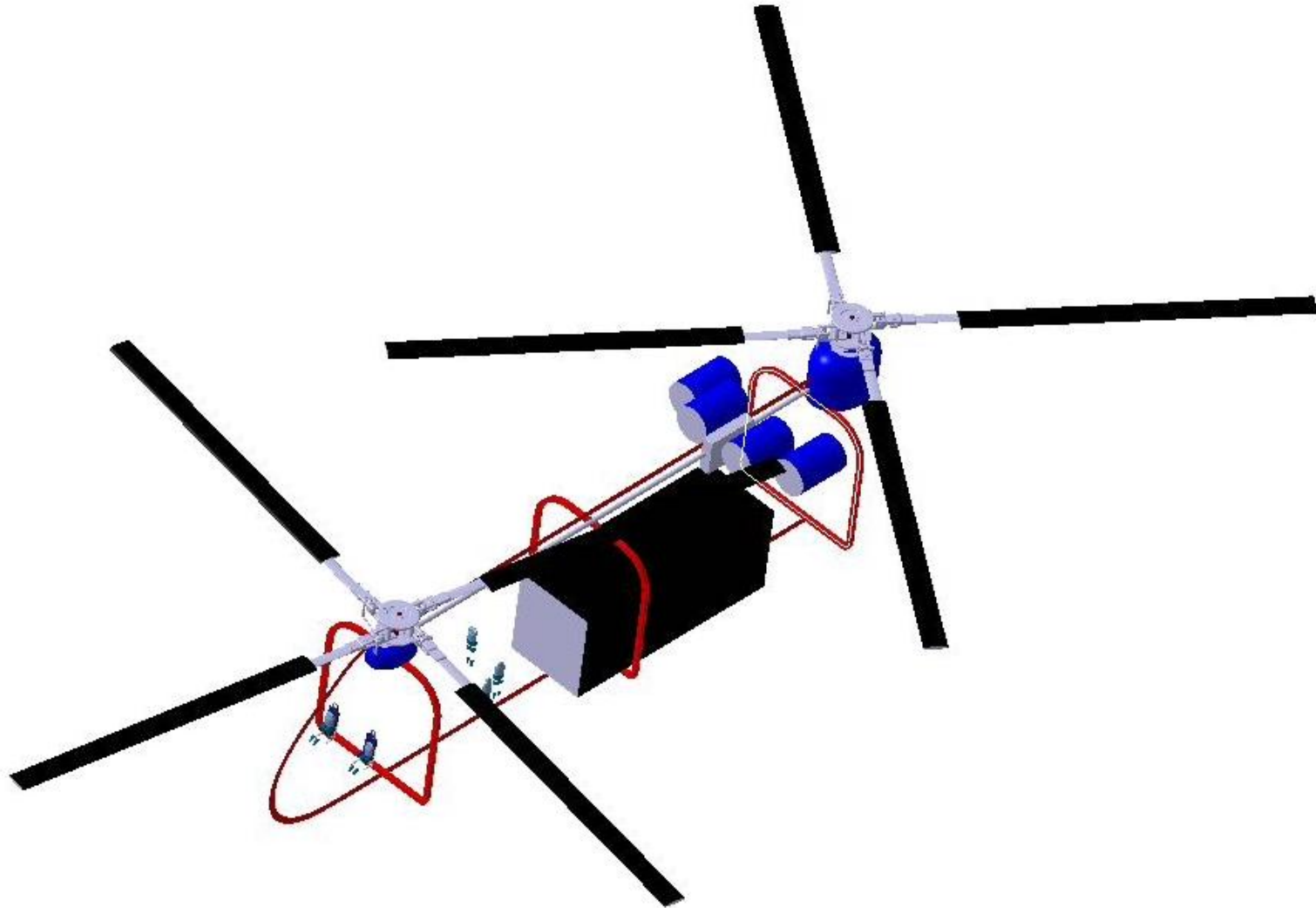
12.1 3 View



12.2 Isometric View



12.3 Internal Layout



13 References

- [1] Systems Engineering Fundamentals, Defense Acquisition University, Fort Belvoir, VA, January 2001.
- [2] JVX Technology Assessment, Appendix D – **General Parasite Drag Methodology**, 1984.
- [3] Technical Manual: **Operator’s Manual for Army CH-47D Helicopter**. Headquarters, Department of the Army. 31 January 2003.
- [4] Prouty, R.W.: **Helicopter Performance, Stability, and Control**. Krieger Publishing Company, Inc. Malabar, Florida, 1986.
- [5] Leishman, J.G.: **Helicopter Aerodynamics**. Cambridge Aerospace Series. Cambridge University Press. 2000.
- [6] ADS TN 68-1. Bellaire, R., Bousman, W.: **A Study of the Army Hot Day Design Hover Criterion**. US Army Aviation Systems Command. St. Louis, Missouri. August 1970.
- [7] AMCP 706-201: **Engineering Design Handbook**. Helicopter Engineering. Part One – Preliminary Design. Headquarters, U.S. Army Material Command. 1974.
- [8] AMCP 706-202: **Engineering Design Handbook**. Helicopter Engineering. Part Two – Detail Design. Headquarters, U.S. Army Material Command. 1976.
- [9] Johnson, W.: **Helicopter Theory**. Dover Publications, Inc. New York. 1980.
- [10] Mavris, D.N., Roth, B.: **A Methodology for Robust Design of Impingement Cooled HSCT Combustor Liners**. 35th Aerospace Sciences Meeting and Exhibit, Reno, NV, Jan 6-9, 1997.
- [11] Drela, M., **XFOIL: An Analysis and Design System for Low Reynolds Number Airfoils**. Conference on Low Reynolds Number Airfoil Aerodynamics, University of Notre Dame, June 1989.
- [12] <http://www.ena.eumd.edu/AGRC/Aero/history.html>
- [13] Hanson, : **The ideal rotor**.
- [14] Schrage, D. P.: **Rotorcraft Design II**. Class Notes. Georgia Institute of Technology, Spring 2005.
- [15] USAAVRADCOM-TR-80-D-11: **Heavy Lift Helicopter – Prototype Technical Summary**. Boeing Vertol Company, Philadelphia, PA, April 1980.
- [16] Amer, K. B., Tapscott: **Studies of the Lateral-Directional Flying Qualities of a Tandem Helicopter of Forward Flight**, NASA Report 1207.
- [17] McEneaney, D.M.: **Draft, Aeronautical Design Standards, Structural Design Criteria for Rotary Wing Aircraft**. U.S. Army Systems Command. St. Louis, MO. November 1985.
- [18] Rosenstien, H., Stanzone, K. A., and Wisniewski: **User’s Manual for HESCOMP, The Helicopter Sizing and Performance Computer Program**. Boeing Vertol Company, D210-10699-2, September 1973.
- [19] USAAMRDL-TR-77-41: **Heavy Lift helicopter – Advanced Technology Component Program – Rotor Blade**. Boeing Vertol Company. Philadelphia, PA, September 1977.
- [20] <http://198.65.138.161/military/systems/aircraft/v-22-propulsion.htm>
- [21] Aviation Week & Space Technology: **Gas Turbine Engines – Outlook/Specifications**. January 19, 2004.
- [22] Kish, J.: **Vertical Lift Drive System Concept Studies Variable Speed/Two-speed Transmissions**. US ARMY RESEARCH LABORATORY. 2002.
- [23] Mishke, S.: **Mechanical Engineering Design**. 1989.